Doppler Wind Lidar From UV to NIR: A Review With Case Study Examples

Mingjia Shangguan[1], Jiawei Qiu[2], Jinlong Yuan[3], Zhifeng Shu[2], Lingfeng Zhou[1] and Haiyun Xia[2,3,4]*

[1]*State Key Laboratory of Marine Environmental Science, College of Ocean and Earth Sciences, Xiamen University, Xiamen, China,* [2]*School of Atmospheric Physics, Nanjing University of Information Science and Technology, Nanjing, China,* [3]*School of Earth and Space Science, University of Science and Technology of China, Hefei, China,* [4]*Hefei National Laboratory for Physical Sciences at the Microscale, Heifei, China*

Doppler wind lidar (DWL) uses the optical Doppler effect to measure atmospheric wind speed with high spatial-temporal resolution and long detection range and has been widely applied in scientific research and engineering applications. With the development of related technology, especially laser and detector technology, the performance of the DWL has significantly improved for the past few decades. DWL utilizes different principles and different tracers to sense the wind speed from the ground to the mesosphere, which leads to the difference in choosing the laser working wavelength. This article will review the working wavelength consideration of DWL, and typical DWLs will present from ultraviolet to near-infrared, after which three typical applications will be shown.

Keywords: wind lidar, Doppler, direct detection, coherent detection, single-photon detector

INTRODUCTION

Lidar has a wide range of applications in atmospheric research, including the characterization of atmospheric aerosol particles (Xia et al., 2015), clouds and visibility (Yu et al., 2017), the concentration of various trace gases such as carbon dioxide (Yu et al., 2021), water vapor (Browell et al., 1979), and atmospheric temperatures (Xia et al., 2014). This article will focus on the Doppler wind lidar (DWL) that utilizes the Doppler effects to remote sensing the atmospheric wind speed. The overviews of DWL principles, techniques, and applications can be found in books or review articles (Werner, 2005; Weitkamp, 2006; Banakh and Smalikho, 2013; North et al., 2014; Reitebuch and Hardesty, 2021). This article will introduce the typical DWLs from the perspective of working wavelengths, with a particular focus on the latest DWL systems and their applications.

Different types of wind lidars with the wavelength from ultraviolet (UV) to near-infrared (NIR) allow measurements in different altitude regions of the atmosphere from the atmospheric boundary layer (ABL) with high aerosol content to the upper troposphere, stratosphere, and even mesosphere with molecules as backscattering targets. As coherent Doppler wind lidar (C-DWL) relies on the measurement of the spectrally narrowband aerosol and cloud returns, C-DWL can measure the wind speed in the aerosol-rich ABL. Whereas, the direct-detection wind lidar (D-DWL) can detect both narrowband backscattering and broadband signal, and it can measure the atmospheric wind speed from the ground to mesosphere.

D-DWLs rely on the measurement of the signal intensity or the number of photons, which makes a good use of one or more narrowband filters and determines the Doppler frequency that shifts from the transmitted signal strength through this filter, called the edge technique, or from the radial-angular distribution or spatial movement of the interference patterns (fringes) of an interferometer, called the fringe imaging technique or interferometric techniques (Weitkamp, 2006). The most

common D-DWL lidar uses the powerful commercial Nd:YAG laser that can emit the laser at 1,064, 532, and 355 nm with the feature of high robustness and reliability. Benefiting from the development of single-photon detector and fiber laser at NIR, the micro-pulse D-DWL at 1.5 μm has recently been developed (Shangguan et al., 2016; Xia et al., 2016). As the single-photon sensitivity in detection, long-range wind detection can be realized with a low-power laser and a small-aperture transceiver. Originally, DWLs were large heavy instruments, but owing to the use of components developed for use in optical fiber communication at 1.5 μm, lidars have been improved in compactness, reliability, and ease of use.

Whereas, the fundamentals of C-DWL are based on heterodyne techniques. C-DWL not only measures the intensity of backscattering signal but also additionally measures the phase and frequency of the backscattered signal. In order to acquire the high coherent mixed-frequency efficiency, C-DWL uses higher wavelength than D-DWL, from the NIR even to mid-infrared. Especially, with the development of eye-safe fiber-based C-DWLs at 1.5 μm starting in the mid-1990s, the first commercially available products became available about 15 years later. As C-DWLs rely on the measurement of the spectrally narrowband aerosol and cloud backscattering signal, they can, in principle, achieve higher precision for the same signal-to-noise ratio (SNR) as D-DWL relies on the backscatter of broad bandwidth molecular signals. In fields like aviation safety and aerodynamics design, high spatial-resolution wind detection is highly demanded. However, improving the spatial resolution of C-DWL is generally more difficult than that of D-DWL. Since the spatial resolution enhancement of DWL is generally achieved by reducing the pulse duration of the transmitted laser according to the basic lidar equation, it inevitably induces the sacrifice of other properties, such as the SNR, maximum detection range, and real-time data processing of C-DWL. To solve this problem, various methods have recently been developed in the C-DWL, including a joint time–frequency analysis (JTFA) method (Wang et al., 2018), Golay coding technique (Wang et al., 2019), and differential correlation pair (DCP) technique (Zhang et al., 2021). Apart from the derived LOS wind speeds, C-DWL also provides a spectrum information that has been applied for precipitation observation (Wei et al., 2019), cloud identification (Yuan et al., 2020), and other applications (Wei et al., 2021).

In addition to the derived LOS wind speeds, the backscattered intensities, SNR, or carrier-to-noise ratio (CNR) are derived from Doppler wind lidars and used for atmospheric scene classification similarly as for backscatter lidars. Thus, the vertical extent and boundaries of aerosol and cloud layers, as well as the height of the ABL, are determined from DWLs (Wang et al., 2021). In addition to the mean component of the wind vector, its turbulent fluctuations around the mean can be derived from DWL measurements with high temporal resolution (Jiang et al., 2021). This is mainly the case for turbulent vertical wind fluctuations, where vertical pointing instruments are used. Also, quantities such as the turbulent energy dissipation rates can be determined with a DWL, and recently, cloud, precipitation, wind shear, and turbulence have been identified by deep analysis on the power spectrum of C-DWL (Yuan et al.,

2020). An excellent review about the measurement and the derivation of turbulent quantities is provided in (Sathe and Mann, 2013) a textbook about coherent DWL (Banakh and Smalikho 2013).

In conclusion, D-DWLs are usually operated at a short wavelength, from UV to visible band, and recently have been expanded to NIR with the application of single-photon technology, whereas C-DWLs operate at a longer wavelength from NIR to even mid-NIR to guarantee the mixing efficiency. By using the wavelength in NIR, various commercial C-DWLs are applied for wind detection in the aerosol-rich ABL and cloud movement in the boundary layer and troposphere. Whereas, D-DWL operated UV band allows the determination of wind speeds in the troposphere, stratosphere, and even up to the mesosphere based on molecular backscatter. Thus, the D-DWL offers a unique capability to measure higher-altitude winds. Various applications have been carried out with DWLs, especially with the improvement of spatial resolution and deep analysis of power spectrum, and the application areas are expanded from atmospheric research and wind energy to grave wave detection, turbulence identification, and even precipitation detection. Therefore, this article will focus on recent advances of DWLs from the perspective of working wavelength and show three typical applications of DWLs.

This article is originated as follows. Firstly, the consideration of DWL wavelengths is summarized, and the principle of wind detection is taken into account. Secondly, recent advances in DWL from UV to NIR band are presented, with a focus on typical wind lidar systems, followed by a discussion of the trends of DWL at different wavelengths. Then, the applications of DWL are summarized. Finally, discussion and conclusions are provided.

WORKING WAVELENGTH CONSIDERATIONS

The choice of the wavelength of DWLs is first and foremost related to its detection principle. There are two fundamental principles used to determine the Doppler shift. In the first method, which is direct detection, an optical frequency discriminator or spectrum analyzer converts the optical frequency change into a change in power or the spatial distribution of power. In these direct detection lidar systems, the return optical signal is filtered or resolved into its spectral components prior to detection. In the second method, no optical frequency discriminator or spectrum analyzer is used. Instead, the backscattering signal is optically mixed with a local oscillator laser, and the resulting beat-signal frequency is, except for a fixed offset, the Doppler shift due to the moving particles.

As shown in **Table 1**, NIR is preferred to obtain a better coherent mixed-frequency efficiency for C-DWLs. C-DWLs operated at shorter wavelengths require highly accurate optical instrument surfaces and are more sensitive to the atmospheric refractive index changes and atmospheric turbulence, both of which deteriorate the mixed-frequency efficiency. However, the D-DWLs are operated from UV to NIR by measuring the broadband molecular backscatter or narrowband Mie

TABLE 1 | Differences in the selection of working wavelength between C-DWLs and D-DWLs.

Detection principle	Direct detection				Coherent detection		
	–				–		
Wavelength	355 nm	532 nm	589 nm	1.06 μm	1.5 μm	2 μm	10.6 μm
Laser	Nd:YAG	Nd:YAG	Dye laser	Nd:YAG	Raman; OPO; Nd: YAG; Er	Tm:YLuAG; TmH:YAG	CO_2 gas laser
Tracer	Aerosol and molecule	Aerosol and molecule	Sodium atom	Aerosol and molecule	Aerosol	Aerosol	Aerosol
References	Xia et al. (2012)	Wu et al. (2003)	She and Yu (1994)	Xia et al. (2007)	Phillips et al. (1997)	Henderson et al. (1991)	Marinov et al. (1996)

backscatter. Since D-DWLs can utilize the molecular backscatter, by taking the advantage of the λ^{-4} dependence of the molecular backscatter, D-DWL offers a unique capability to sense the wind speed in the stratosphere, even up to the mesosphere.

DWL mainly comprises a transmitter, receiver system, data acquisition system, and data analysis system. The essential components of the DWL transmitter are the laser. From UV to NIR, the gain media of laser is distributed over three bands, namely, 1.0, 1.5, and 2.0 μm, in which the laser source could obtain high-pulse energy. Due to its robustness and reliability, the most common source used in D-DWL is a commercial Q-switched Nd:YAG laser that operates at the wavelengths of 1,064, 532, and 355 nm. Among the D-DWLs, solidum D-DWL is a Na doppler resonance fluorescence lidar and assembles with yellow 589-nm laser to excite sodium atoms in the mesopause region. Moreover, D-DWL operated at 1.5 μm is developed by the single-photon detector at NIR. In principle, the SNR of lidar is dominated by the product of laser power and the telescope area. Although the detector used in a lidar finally decides the quality of the raw data, its contribution is often neglected. Since the commercial InGaAs avalanche photodiode suffers from low efficiency (about 18%), high noise (a few kHz) due to impurities, and defects of the cathode material, the wavelength at 1.5 μm is not applied for D-DWL. Recently, with the development of a single-photon detector at 1.5 μm, including frequency up-conversion detector (UCD) and superconducting nanowire single-photon detector (SNSPD), the wavelength of 1.5 μm was applied in D-DWL.

In order to achieve high mixing efficiency, C-DWL applied laser with the longer wavelength at 1.06, 1.5, 2.0, and 10.6 μm. Among those wavelengths, the most mature wavelength is at 1.5 μm, due to its eye safety, compact size, flexible arrangement, and mature fiber component technology from the telecommunication industry.

For the full-time automatic operation of lidars in the field, in addition to the laser and detector, the issues of atmospheric transmittance (Ångström, 1929), solar background noise, and maximum permissible exposure should be taken into accounts. Comparatively, the wavelength of 1.5 μm shows the highest maximum permissible exposure in the wavelength ranging from 0.3 to 10 μm (Institute and America, 2007). What is more, in contrast with UV and visible systems, 1.5-μm lidars
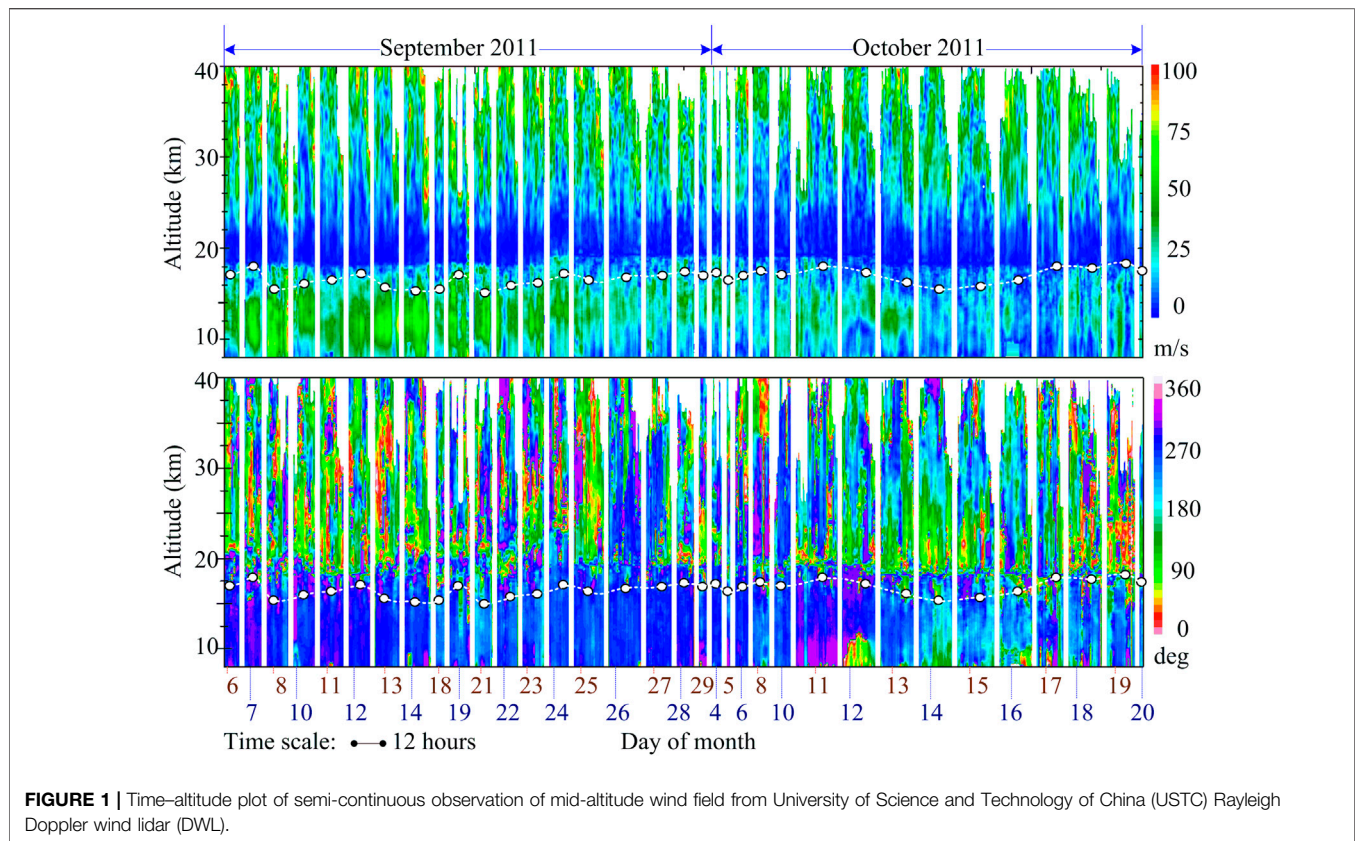
suffer lower atmospheric attenuation, minor disturbance from Rayleigh scattering, and weaker sky radiance. In addition, it is important to avoid the absorption of the transmitted laser by other molecular atmospheric components, such as water vapor, carbon dioxide, etc.

DIRECT-DETECTION DOPPLER WIND LIDAR FROM 355 nm TO 1.06 μm

In the altitude range from the upper troposphere to the stratosphere, where the Mie backscattering signal is usually weak, Rayleigh DWL is the unique wind remote-sensing instrument with high spatial and temporal resolution. Global wind field measurements throughout the troposphere and lower stratosphere are essential for understanding and predicting the future state of the earth-atmosphere system. High accuracy and real-time wind measurement will also address some vital needs such as Air Force operations, hurricane tracking, epidemic prevention, and potential chemical biological release trajectory prediction.

Although the first D-DWL has been demonstrated about 40 years ago, there are only a few reports of stratospheric wind measurements using Rayleigh D-DWLs. The wind detection up to 50 km was first realized using a double-edge Fabry–Perot interferometer (FPI) as the frequency discriminator at the Observatory of Haute Provence (OHP), France (Chanin et al., 1989). A similar Rayleigh lidar based on a single FPI was developed for wind measurement to an altitude near 60 km at the Arecibo Observatory (Tepley, 1994). Later, the pressure-scanned FPI was replaced by a molecular iodine filter (Friedman et al., 1997). Both FPI and iodine filter were reported to mid-altitude wind measurement at the ALOMAR research station near Andenes, Norway (Rees et al., 1996). Recent experiments demonstrated its ability of measuring the wind and temperature up to 80 km. The working wavelength of all literature cited in the last paragraph is 532 nm.

Goddard Lidar Observatory for Winds (GLOW) mobile DWL was developed using double-edge FPI and frequency-tripled Nd: YAG laser at 355 nm at NASA Goddard space flight center (Gentry et al., 2000). A similar mobile Rayleigh DWL was built at the University of Science and Technology of China

FIGURE 1 | Time–altitude plot of semi-continuous observation of mid-altitude wind field from University of Science and Technology of China (USTC) Rayleigh Doppler wind lidar (DWL).

(USTC) (Xia et al., 2012). The semi-continuous observed result of mid-altitude wind field from USTC is shown in **Figure 1**.

The exploitation of global wind profiling by the use of spaceborne wind lidars just started with the launch of Aeolus in August 2018 (Reitebuch, 2012). The Aeolus mission is supposed to improve the quality of weather forecasts and the understanding of atmospheric processes. The commonly used double-edge technique was also applied on Aeolus.

The Doppler shift carried by Mie or Rayleigh backscattering can be determined directly using high-resolution frequency discriminators, such as FPI (Xia et al., 2007), iodine absorption filter (Liu et al., 2002), Fizeau interferometer (McKay, 2002), Mach–Zehnder interferometer (Bruneau et al., 2004), and Michelson interferometer (Cézard et al., 2009). In the ADM-Aeolus payload ALADIN, a Fizeau interferometer and a double-edge FPI were used to analyze the Mie and Rayleigh backscattering, respectively (Paffrath et al., 2009; Reitebuch et al., 2009).
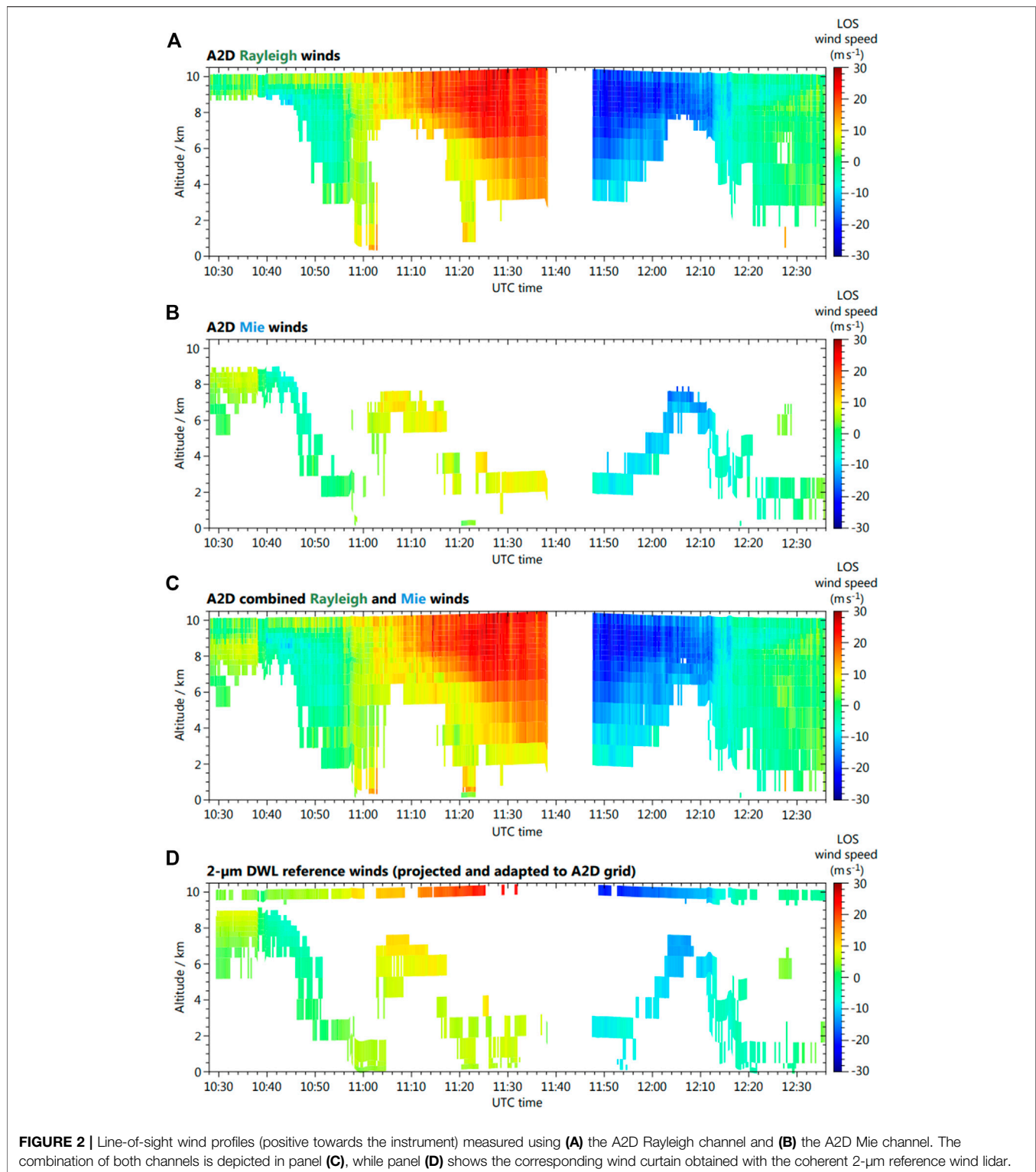
Mobile Rayleigh D-DWL

A mobile Rayleigh DWL based on the double-edge technique was developed for mid-altitude wind observation at USTC (Xia et al., 2012; Shangguan et al., 2015). The whole lidar system is integrated into the first truck. Wind observation over 2 months was carried out in Urumqi (42.1°N, 87.1°E), northwest of China, which demonstrates the stability and robustness of the system. For the first time, the quasi-zero wind layer and dynamic evolution of high-altitude tropospheric jet were observed based on Rayleigh DWL in Asia.

Spaceborne D-DWL

The designs and measurement principles of Spaceborne wind lidar on Aeolus have been extensively specified in previous publications that have described the satellite (Stoffelen et al., 2005; Reitebuch, 2012; Lux et al., 2019) and airborne demonstrator A2D (Paffrath et al., 2009; Reitebuch et al., 2009), respectively. Satellite DWL ALADIN (atmospheric laser Doppler instrument) on Aeolus consists of a frequency-stabilized, ultraviolet laser transmitter, a Cassegrain telescope, front optics, and a dual-channel receiver. The latter is composed of a Fizeau interferometer and sequential FPI for analyzing the Doppler frequency shift from particulate and molecular backscatter signals, respectively. The validation of the instrument performance and retrieval algorithms was conducted by comparison with DLR's coherent wind lidar that was operated in parallel, as shown in **Figure 2**, which indicates a systematic error of the A2D line of sight winds of less than 0.5 m/s and random errors from 1.5 (Mie) to 2.7 m/s (Rayleigh) (Lux et al., 2018). After the launch of Aeolus, several ground-based C-DWLs have been deployed to verify the wind observations from Aeolus (Wu et al., 2021).

FIGURE 2 | Line-of-sight wind profiles (positive towards the instrument) measured using **(A)** the A2D Rayleigh channel and **(B)** the A2D Mie channel. The combination of both channels is depicted in panel **(C)**, while panel **(D)** shows the corresponding wind curtain obtained with the coherent 2-μm reference wind lidar.

D-DWL at 589 nm

In addition to the Mie scattering and Rayleigh scattering signals, there is another direct detection lidar based on fluorescence backscattering for wind speed detection in the mesopause region.

She and Yu (1994) at Colorado State University implemented narrow-band sodium wind lidar, which used a dye laser at a wavelength of 589 nm to induce the fluorescence in the mesopause region (80–105 km) (She and Yu, 1994; Krueger

et al., 2015). This lidar was then upgraded to 24-h continuous observation in 2002. Subsequently, another research group from the University of Illinois at Urbana-Champaign developed a Na wind/temperature lidar for simultaneous detection of Na density, atmospheric temperature, and vertical winds between 84 and 100 km (Gardner et al., 1995).

The research groups of Li at USTC following the CSU sodium fluorescence Doppler lidar developed a narrowband high-spectral resolution sodium temperature/wind lidar in 2012 (She et al., 2002; Li et al., 2012). The sodium density, temperature, zonal wind, and gravity wave (GW) zonal momentum flux were observed by the USTC Na doppler lidar between January 2012 and December 2016 at Hefei, China (Li et al., 2018). The research groups of Cheng at Wuhan Institute of Physics and Mathematics (WIPM), Chinese Academy of Sciences, developed a solid-state sodium Doppler lidar for simultaneous wind and temperature measurement at YanQing Station, Beijing, in 2017 (Xia et al., 2017).

DIRECT-DETECTION DOPPLER WIND LIDAR AT 1.5 μm

D-DWL Based on Up-Conversion Single-Photon Detector

In contrast to earlier DWLs based on free-space optics, the use of fiber-optic elements and integrated devices at working wavelengths of 1.5 μm offers practical advantages, including mechanical decoupling and remote installation of the subsystems, simplification of configuration and alignment, and enhancement in coupling efficiency and long-term stability. In 2016, the single-photon D-DWL at 1.5 μm was developed by using an UCD (Shangguan et al., 2016; Xia et al., 2016). The UCD upconverts photons at a communication band to visible photons when quasi-phase matching is achieved in a periodically poled lithium niobate waveguide. Then single photons at 1.5 μm can be counted by using a Si avalanche photodiode with high efficiency, low noise, and less afterpulsing.

The commonly used double-edge technique was applied on 1.5-μm D-DWL. The transmission curve and reflection curve of a single-channel fiber-FPI were applied to construct the double-edge. The double-edge technique is implemented by using a convert single-channel FPI and a single UCD, incorporating a time-division multiplexing method. The transmitted signal through the FPI is coupled into a UCD, while the reflected signal is timely delayed, after propagating through a circulator and an 8-km polarization-maintaining fiber. By using an optical switch, the transmitted and reflected signals can be directed into the detector alternatively. A D-DWL is operated in a photon-counting mode, thus making it easy to record and process the raw data. Since the lidar adopts an all-fiber and polarization-maintaining architecture, the accuracy and stability of its system are improved substantially.

The continuous 48-h detection results of the single-photon DWL are displayed in **Figure 3** with 1-min temporal resolution and 30-m spatial resolution. Comparing the simultaneous measurement of the single-photon lidar and another installed

ultrasonic anemometer, the difference between both is counted with an average variation of 0.05 m/s in wind speed, −0.84° in wind direction, and the standard deviation of 1.04 m/s in wind speed, and 12.3° in wind direction.

D-DWL Based on Superconducting Nanowire Single-Photon Detector

The conventional double-edge DWL utilizes the double-channel FPI, which leads to complex systems, high operating costs, and the challenge of repeated calibration. To solve those challenges, a proposal of double-edge wind lidar based on dual-frequency laser pulse arose (Shangguan et al., 2017). One of the frequencies (f_s) of the dual-frequency laser is in the rising edge of the FPI transmission curve, while another one (f_0) is in the falling edge. When the Doppler shift happens in atmospheric backscattering signals, the difference of transmission of the dual-frequency signal could be observed, which enables us to discriminate the frequency.

The D-DWL utilizes the SNSPD with the highest signal/noise ratio at 1,550-nm wavelength. It owns over 60% quantum efficiency and less than 300 Hz dark count and enables a high signal/noise ratio detection by the wind lidar. A continuous atmospheric observation experiment is performed under dual-frequency DWL, and the wind field evolution process in the ABL before thunderstorms is captured.

COHERENT DOPPLER WIND LIDAR

C-DWL at 1.06 μm

In 1985, Kane et al. (1987) from Stanford University developed a 1.06-μm C-DWL based on Nd:YAG laser, using a flash lamp pumped (FLP) laser with an amplified pulse power of 2.3 kW, which conducted the observation of 600-m wind field and 2.7-km high cloud. Another research group led by Kavaya et al. (1989) also successfully developed a 1.06 C-DWL system with 8-mJ pulse energy at 1-μs width and 5-mJ energy at 0.5-μs width at 10-Hz repetition frequency and detected the horizontal wind field at 3.75 km distance. Subsequently, under the cooperation of Coherent Technology Inc. NASA George C. Marshell Space Flight Center (MSFC) and NASA Langley Research Center (LaRC), the C-DWL system was upgraded with 1-J pulse energy and 10-Hz repetition frequency to ensure the launching and landing safety of STS Discovery OV-103 spacecraft in Kennedy Space Center (KSC), and the wind field detection from ground to 26-km height was conducted (Hawley et al., 1993). Due to the eye safety considerations, 1.06 μm was gradually replaced by 1.5- and 2-μm bands.

C-DWL at 2.0 μm

The exposable power of a 2-μm laser is four orders larger than 1.06 μm, which shows great superiority to a 2-μm laser in eye safety. Out of consideration for safety, the 2-μm all-solid-state C-DWL system has wider applications.

The first 2.09-μm C-DWL with a Tm, Ho:YAG laser of FLP was developed by the research group of Henderson et al., (1991) (Suni
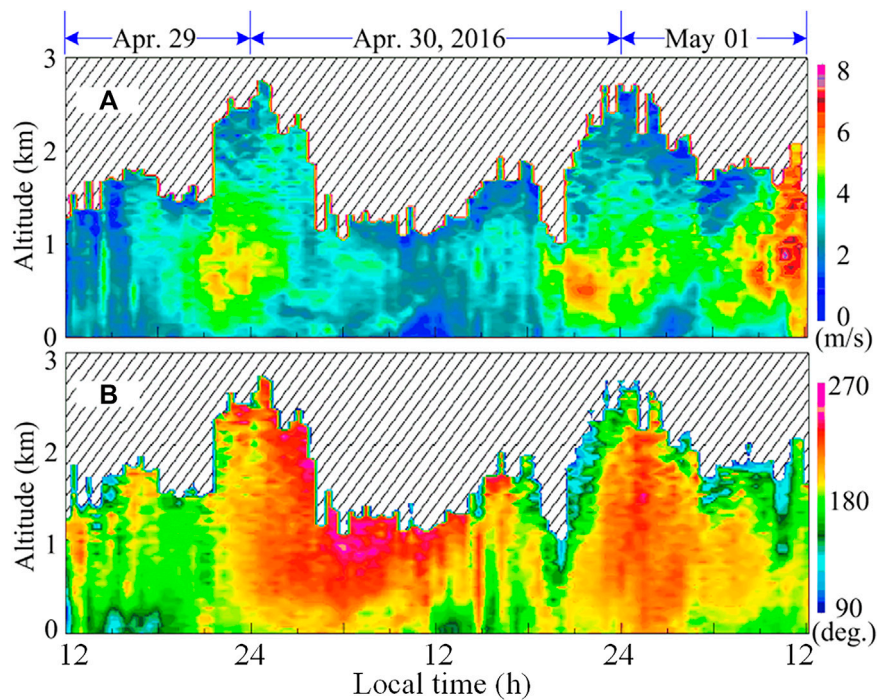
FIGURE 3 | Forty-eight-hour observation of atmospheric wind and visibility. **(A)** Wind speed and **(B)** direction.

and Henderson, 1991). In the following year, Suni and Henderson (1991) further optimized the lidar system and accomplished the wind field detection at 20-km distance and hard subject detection at 145 km with 2-μm laser, 20-mJ pulse energy, and 20-cm-diameter telescope (Henderson et al., 1993). Based on this technique, the CTI Company adopted a Tm:YAG laser with a pure semiconductor pump to develop the first 2.01-μm onboard C-DWL with an InGaAs photodiode, 1.8-mJ pulse energy, 0.5-μs width, and 75-m distance resolution. It has been utilized to conduct an onboard detection in NASA Boeing 737 aircraft in 1994. The wind shear and microburst were observed (Targ et al., 1996). With a promoted design, the accuracy of the onboard detection of wind velocity reached 10 cm/s in 1996. The NOAA conducted a high-resolution wind field detection with the highest spatial resolution of 30 m based on shipboard (Wulfmeyer et al., 2000) and land-based system (Newsom and Banta, 2003) using the C-DWL of a similar design. With the promotion of 2-μm laser and data-processing techniques, Lockheed Martin Coherent Technologies, Inc. has commercialized the WindTracecr series C-DWL system (Gatt et al., 2015).

The NASA and United States Air Force applied a C-DWL system with high-pulse energy and 100-Hz repetition frequency in airborne detection of CAT and surrounding wind field. Kavaya et al. (2014) from NASA reported the measurement results of a 2-μm C-DWL with 250-mJ pulse energy, 10-Hz repetition frequency, and 180-ns width.

In 2010, the research group from HIT constructed a 2-μm C-DWL with 2-mJ single-pulse energy, 100-Hz repetition frequency, 300-ns width, and a telescope of 150-mm diameter,

to verify the theoretical model, optical signals at 2 μm, and signal-processing algorithm. The heterodyne signals at 16- and 96-m distance are gained (Bu et al., 2015).

Regarding the complete differentiation and statistical theory, the research group from BJUT built a common error analytical model of the synthesis horizontal wind speed and direction of the spaceborne 2-μm C-DWL and gave a detailed analysis of the key technology (Bu et al., 2015).

C-DWL at 1.5 μm

Entering the 20th century, with the fiber-optic communication technique development, the 1.5-m C-DWL with a compacter internal structure and higher luminance efficiency has become an emerging area in the lidar field.

From the birth of the first CO_2 C-DWL, Lockheed Martin Coherent Technologies (LMCT) has always been devoted to C-DWL technique development. It has commercialized one 2-μm WindTracer C-DWL in 2002, while the current WindTracer series has been upgraded into 1.617-μm Er:YAG laser-based lidar. NASA applied the WindTracer system in the detection of wind shear and CAT and subsequently modeled and predicted the aircraft vortices in 2009, at the Denver International Airport (Proctor and Hamilton, 2009).

The single-pulse energy of 3 mJ requires extremely high requirements of the laser performance and optical element quality, and thus, the lidar is fragile and has a short life span resulting in low applicability (Prasad et al., 2016). To solve that, NASA developed another all-fiber Windimager C-DWL system based on Er glass fiber laser.

Spuler et al. (2011) from NCAR conducted an aircraft forward-turbulence measurement on August of 2010 using a continuous-wave (CW)-based C-DWL. The telescope of 50-mm diameter focusing 30 m ahead of the aircraft was installed in the nacelle of the aircraft wing. Compared with the flight speed collected by the pitot tube of the aircraft, the accuracy of the lidar wind speed detection is 0.052 m/s higher.

Engin et al. (2016) from the world-famous optoelectronic company FiberTek Inc. numerically simulated the turbulence and wake vortices of Boeing 747 aircraft and conducted a real detection using their self-developed C-DWL prototype, which works at 1.55-μm operation wavelength and 2.5-kHz linewidth. When the repetition frequency is 20 kHz, the relative intensity noise (RIN) is lower than −140 dBc/Hz and the AOM frequency shift will be 55 MHz. After the utilization of a second-order laser amplifier system, the output laser pulse energy reaches 120 μJ with a 25-kHz repetition frequency and 800-ns width.

Mitsubishi Electric Corporation (MEC) has always been devoted to the C-DWL development since the end of the 1990s (Kameyama et al., 2013). Regarding the 1.53-μm semiconductor seed laser, MEC's Asaka et al. (1998) applied an Er, Yb:glass laser amplifier to increase its single-pulse energy to 2.5 mJ in 1998, which is able to detect horizontal distance at 800 m with a telescope at the diameter of 600 mm.

Later, Yanagisawa et al. (2001) upgraded the Er, Yb:glass laser into 1.54 μm, one with 10.9-mJ single-pulse energy, 228-ns width, and 15-Hz repetition frequency, and it was used in the wind field detection at 5-km distance measured by a telescope of 100-mm diameter (Asaka et al., 2001). After another upgradation of the 1.54-μm C-DWL system by Fujiyoshi (2007) from MEC, the detection distance reached 10 km, and subsequent field measurements were conducted. The all-fiber system is characterized by its compact internal structure, convenience in installation and maintenance, low cost, and stable system. MEC has reported their research progress of all-fiber C-DWL system in 2002 and introduced their prototype in 2003 (Kameyama et al., 2007), following with the first commercialized LR-05FC (Ando et al., 2008). The upgraded all-fiber C-DWL LR-08FS was applied in Hongkong Airport in 2010 (Chan and Lee, 2012). With the utilization of thick core fiber of 25-μm diameter and second-order laser amplification in LR-05FS, the single-pulse energy reached 179 μJ, which enables the horizontal wind field detection of greater than 10 km. MEC has already owned three product series of all-fiber C-DWL according to their detection distances (Inokuchi et al., 2009a; Inokuchi et al., 2010).

Through the application of the planar lightwave circuit (PLC) technique and second-order laser amplification technique, Sakimura et al. (2013) further amplified the laser output power with a longer detection distance at 30 km. Later in 2014, MEC reported their airborne test result. This system allowed horizontal detection at greater than 9-km distance, which enables CAT detection 30 s in advance (Kameyama et al., 2012; Sakimura et al., 2013).

Subsequently, in 2014, MEC reported the results of airborne experiments with the system (Inokuchi et al., 2009b). At a flight altitude of 12 km, the system achieves a horizontal detection range of >9 km and can be used to detect turbulence in clear skies up to 30 s in advance (Inokuchi et al., 2014).

French Office national d'études et de recherches aérospatiales (ONERA) first reported their 1.5-μm C-DWL in 2008 (Dolfi-Bouteyre et al., 2008), and the measurement of aircraft wake vortices. Considering the stimulated Brillouin scattering effect in the fiber, ONERA self-developed a fiber laser amplifier containing Er, Yb (Canat et al., 2007).

In 2009, ONERA upgraded the first-generation C-DWL system with a three-order pump to amplify the seed laser and a large mode area fiber to suppress the stimulated Brillouin scattering. Its laser energy is increased to 120 μJ to measure the aircraft wake (Dolfi-Bouteyre et al., 2009a; Dolfi-Bouteyre et al., 2009b). Through strain addition in the large-mode area fiber, ONERA further raised the stimulated Brillouin scattering threshold of fiber in 2014 (Renard et al., 2014), consequently succeeding in longer-than-10-km wind field detection with 370 μJ single-pulse energy. Later in 2015, ONERA used multi-amplifiers in parallel to enhance the pulse energy of fiber laser (Lombard et al., 2015b), which completed a 16-km-distance wind field detection with 500-μJ pulse energy (Lombard et al., 2015a). Under the cooperation with Leosphere Company, this laser has been applied in WindCube Series (Thobois et al., 2014; Thobois et al., 2015) and predictions of weather and disaster, and wind shear detection of aircraft and many other field tests were conducted to verify its accuracy (Barbaresco et al., 2015; Hallermeyer et al., 2016).

Leosphere Company was founded in 2004 and has close cooperation with ONERA and the Technical University of Denmark (DTU) with various products, including the land-based WindCube series and wind turbine generator lidar (Wind Iris series) (Thobois et al., 2014; Thobois et al., 2015), that are widely applied in wind power generation (Kigle, 2017), aviation security (Augros et al., 2012), weather broadcasting (Gibert et al., 2012), and air quality monitoring (Chen et al., 2017).

Since the mid of the 1990s, the QinetiQ Company has always focused on replacing CO_2 laser with fiber laser in C-DWL system and succeeded in developing an all-fiber CW C-DWL system at the end of the 1990s. The all-fiber pulsed C-DWL was also developed in 2002 (Karlsson et al., 2000; Harris et al., 2001), applied in wind power generation, and cooperated with DTU (Pearson et al., 2002; Jørgensen et al., 2004; Bingöl, 2005; Smith et al., 2006).

The QinetiQ Company together with DTU developed the first commercialized CW C-DWL system in 2003, with an adjustable-focus telescope to detect the wind at different distances and a unique algorithm to increase wind speed accuracy. The current on-sale product is ZephIR300 that can be installed in land base, vehicles, and wind turbine generators (Pearson et al., 2002).

SgurrEnergy Ltd. developed the Galion series pulsed C-DWL system with DTU, which mainly works on wind field detection and wind energy storage prediction of the wind farm (Gottschall et al., 2014; Wang et al., 2014). In 2013, DTU reported the Galion series measurement results of these years and proved that this system was still stably working, and the current models are G250 and G4000 (Gottschall, 2013).

TABLE 2 | Performance of 1.5-μm C-DWLs.

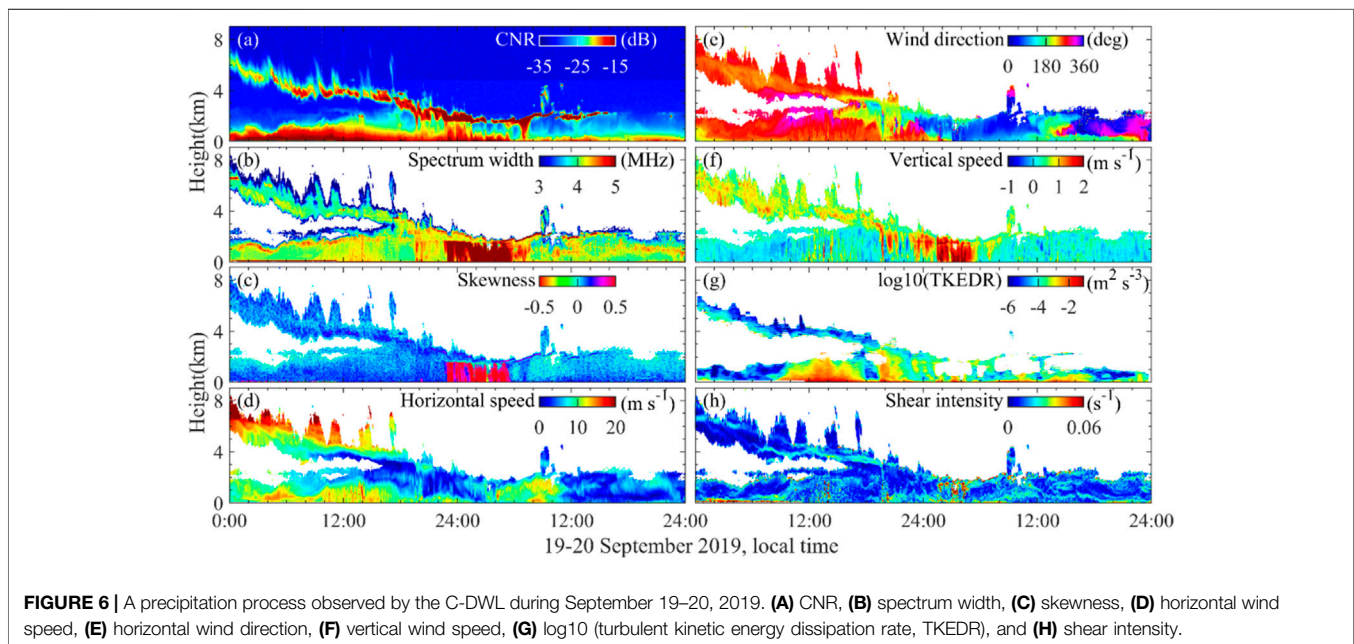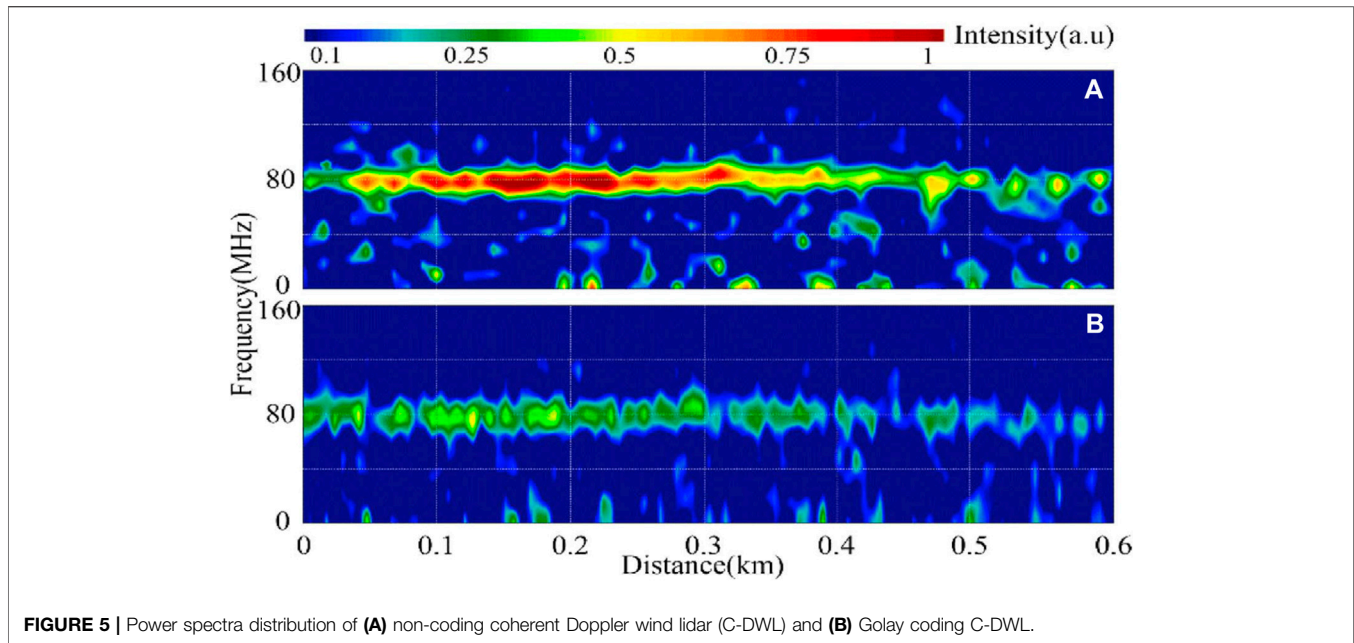| Parameters	λ (μm)	Energy (μJ)	Pulse width (ns)	Prf (KHz)	Detection range (km)	Spatial resolution (m)	Wind speed accuracy (m/s)	Telescope diameter (mm)	References
MEC	1.54	10,900	228	15	5	–	–	100	Yanagisawa et al. (2001)
MEC	1.5	5	500	0.4	1.5	70	–	50	Chan and Lee (2012)
FiberTek	1.5	120	800	25	–	–	–	–	Engin et al. (2016)
SgurrEnergy	1.55	–	–	–	4	–	0.10	–	Gottschall (2013)
ONERA	1.545	500	650	10	16	200	0.19	–	Lombard et al. (2015a)
NASA	1.5	240	400	20	0.4–10	15–60	0.2	101	Prasad et al. (2016)
Leosphere	1.54	–	25–200	–	12–14	25–200	0.1	–	Thobois et al. (2014); Thobois et al. (2015)
LMCT	1.617	2,500 ± 500	250 ± 50	0.75	15	100	1	–	Proctor and Hamilton (2009)
Halo-Photonics	1.562	1,150	–	–	8	–	0.2	–	Pearson et al. (2005)
SIOM	1.540	43	500	10	3	75	0.2	50	Diao et al. (2014)
QinetiQ	1.548	50	24	30	0.5	25	0.5	17.55	Pearson et al. (2002)
OUC	1.55	50	400	10	4	60	0.1	–	Zhai et al. (2017)
USTC	1.548	100	300	15.625	6	60	0.5	80	Wang et al. (2017)
USTC	1.548	300	800	10	10	120	0.3	100	Wei et al. (2020)
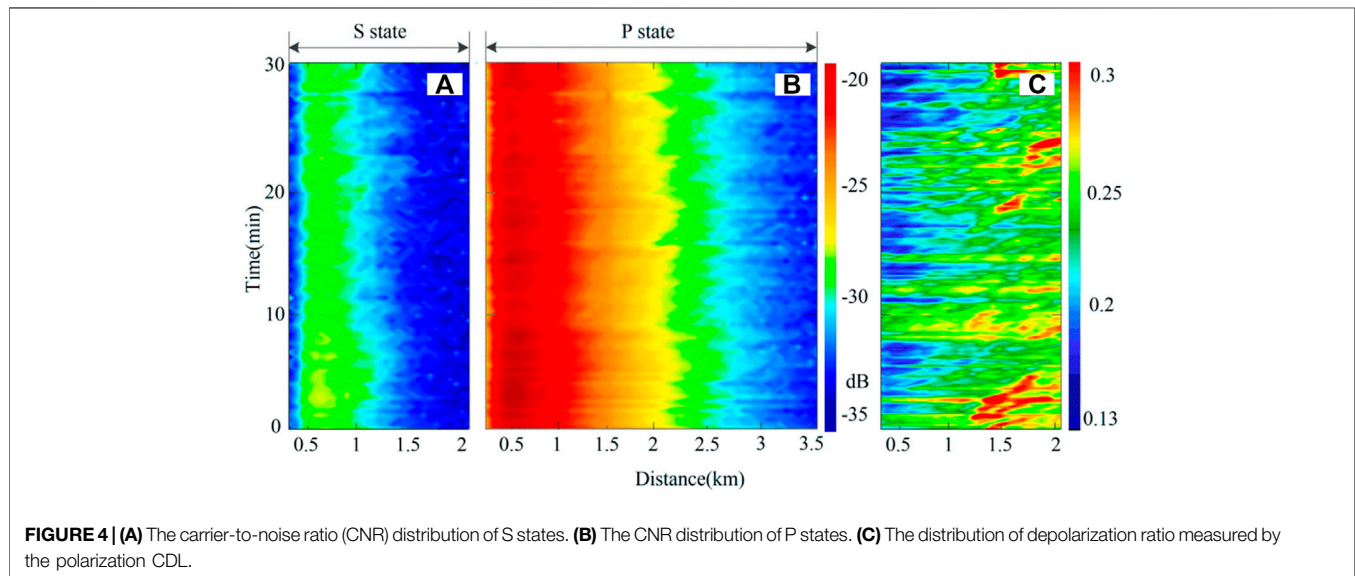
FIGURE 4 | (A) The carrier-to-noise ratio (CNR) distribution of S states. **(B)** The CNR distribution of P states. **(C)** The distribution of depolarization ratio measured by the polarization CDL.

Halo-Photonics Company started developing a C-DWL system based on the CO_2 laser at the end of the 1980s and developed a 1.548-μm pulsed C-DWL system based on fiber elements in 2001 and conducted an atmospheric wind field observation in the following year. In 2004, Halo-Photonics Company developed a high-power laser of 1.562-μm wavelength and 1.15-mJ pulse energy based on the Er, Yb containing laser amplifier (Philippov et al., 2004). Their C-DWL detection distance was improved to 8 km through the application of this laser in the second year (Pearson et al., 2005). It has been used to conduct the measurement of the thunderstorm (Collier et al., 2008), CAT (Hogan et al., 2009), the falling speed of ice cloud crystal (Westbrook et al., 2010), and turbulence dissipation rate (O'Connor et al., 2010).

DTU Wind Energy focuses on relative techniques of the wind energy field and has close cooperation with ZephIR, Leosphere, and many other companies. Due to the strict limit of lidar cost in the wind power generation field, DTU shows high interest in relatively cheap CW C-DWL. The research group of Abari et al. (2014), Pedersen et al. (2014), Abari et al. (2015a), and Abari et al. (2015b) theoretically designed a CW-based C-DWL that could distinguish zonal wind speed. Other groups in DTU are also dedicated to applying cheaper semiconductor lasers to further reduce the cost of lidar production (Rodrigo and Pedersen, 2012; Hu et al., 2014). Then, DTU commercialized the WindScanner series with pulsed and CW mode to detect wind field from 0- to 300-m height. The current product lines of the Halo-Photonics company include the C-DWL detection of visualized and 3D wind fields at near or far distances. Their lidar with the longest detection distance is the Strean Line[XR].

Li et al. (2010) from the 27th Research Institute of China Electronics Technology Group (CETC27) has reported a C-DWL
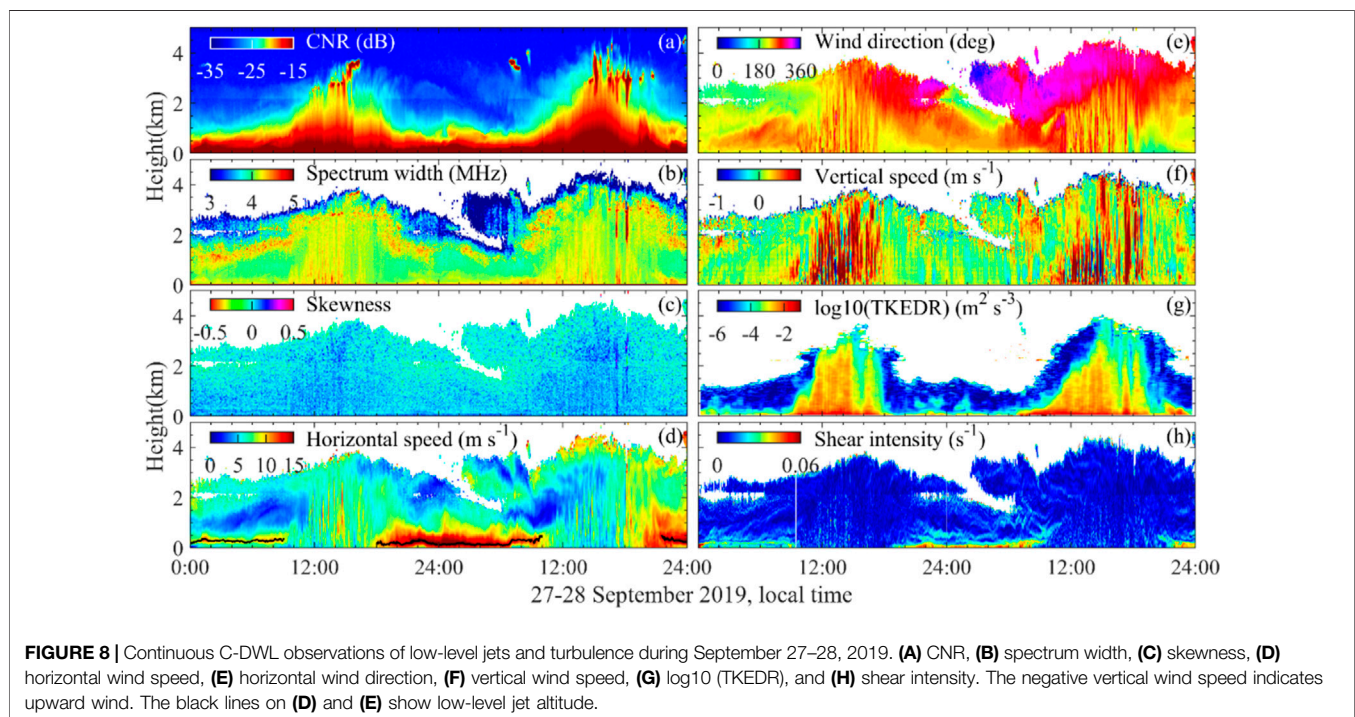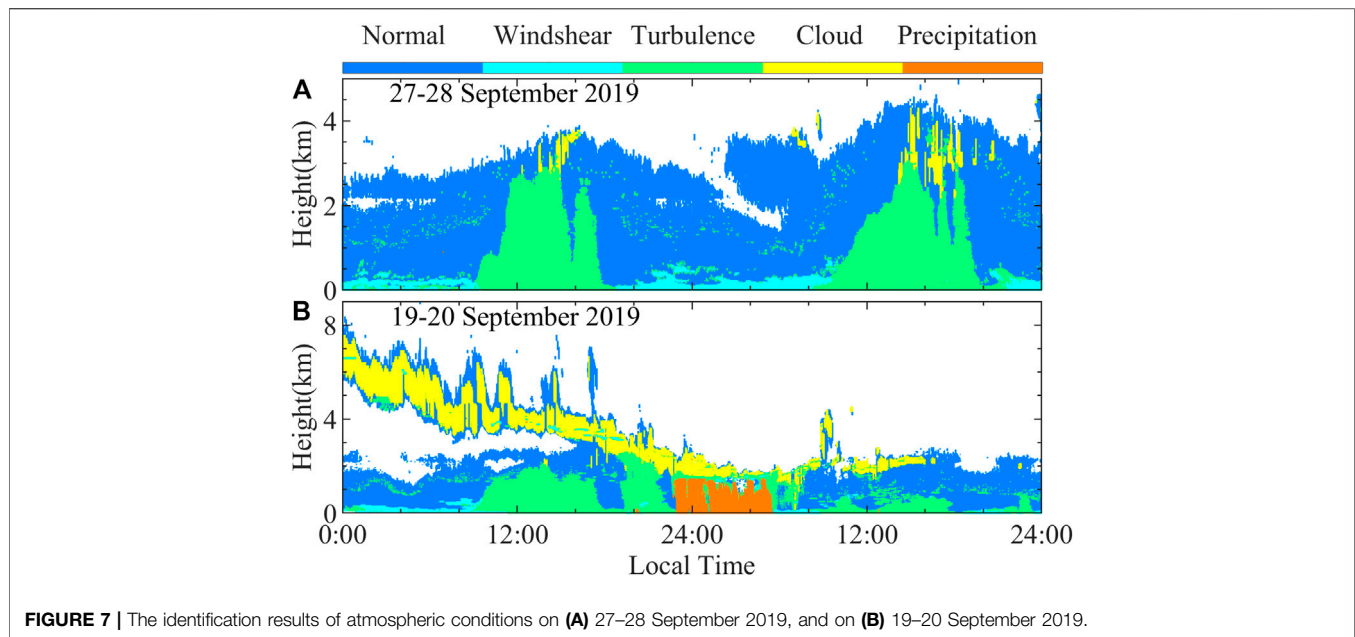
FIGURE 5 | Power spectra distribution of **(A)** non-coding coherent Doppler wind lidar (C-DWL) and **(B)** Golay coding C-DWL.

FIGURE 6 | A precipitation process observed by the C-DWL during September 19–20, 2019. **(A)** CNR, **(B)** spectrum width, **(C)** skewness, **(D)** horizontal wind speed, **(E)** horizontal wind direction, **(F)** vertical wind speed, **(G)** log10 (turbulent kinetic energy dissipation rate, TKEDR), and **(H)** shear intensity.

system based on 1.5-µm CW that could measure wind speed within 200 m. In 2013 and 2015, CETC27 separately reported their developed all-fiber C-DWL system and a comparison experiment at 800-m detection distance with good performance (Pan et al., 2013).

Liu et al. (2012) from the Shanghai Institute of Optics and Fine Mechanics (SIOM) firstly reported their all-fiber 1.538-µm C-DWL and upgraded it in 2014 to conduct detection at the distance of 3 km horizontally and 1.9 km vertically (Diao et al., 2014), and in 2015,

they applied the non-linear least square method to inverse the vector profile of wind speed (Diao et al., 2015).

Wu et al. (2014) from the Ocean University of China (OUC) reported a 1.55-µm C-DWL system in 2014, and it has been applied in wind field observation in the wind farm (Wu et al., 2016; Zhai et al., 2017). Later in 2018, they demonstrated an optimization theory-based conjugated gradient algorithm that inverses the wind field by the velocity replacing the conventional Fourier transform algorithm (Changzhong et al., 2018).

FIGURE 7 | The identification results of atmospheric conditions on **(A)** 27–28 September 2019, and on **(B)** 19–20 September 2019.

FIGURE 8 | Continuous C-DWL observations of low-level jets and turbulence during September 27–28, 2019. **(A)** CNR, **(B)** spectrum width, **(C)** skewness, **(D)** horizontal wind speed, **(E)** horizontal wind direction, **(F)** vertical wind speed, **(G)** log10 (TKEDR), and **(H)** shear intensity. The negative vertical wind speed indicates upward wind. The black lines on **(D)** and **(E)** show low-level jet altitude.

A research group from USTC successfully developed the C-DWL that can simultaneously measure the wind field and depolarization rate of the atmosphere (Wang et al. 2017). Then, they proposed to apply the JTFA and the pulse coding technique to increase the spatial resolution (Wang et al., 2018; Wang et al., 2019). The power spectra distribution of non-coding C-DWL and Golay coding C-DWL are shown in **Figure 5**. An algorithm with accurate noise modeling was then proposed and demonstrated to correct the effect of a time-varying DC noise leakage from the balanced detector, thus enabling a detection range of up to 10 km (Wei et al., 2020). **Table 2** summarizes the performance of 1.5-μm C-DWLs from different organizations and companies around the world.
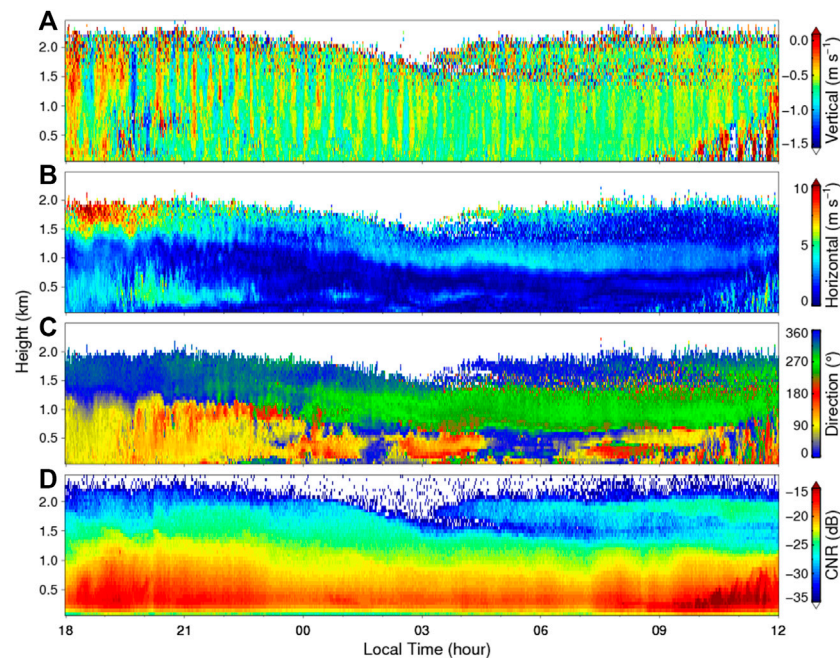
FIGURE 9 | A case of gravity wave process detected by C-DWL. **(A)** Vertical wind, **(B)** horizontal wind speed, **(C)** horizontal wind direction, and **(D)** CNR in vertical obtained by the CDL.

Polarization C-DWL

The coherent lidar usually could not detect the atmospheric depolarization ratio and wind field simultaneously. The research group from USTC has developed a type of all-fiber C-DWL with a single balanced detector to simultaneously measure the wind field and atmospheric depolarization ratio (Wang et al., 2017). Compared with normal C-DWL, this lidar uses a time-division multiplexer module, so that two signals with perpendicular polarization states can be detected alternately. This method needs only one detector to measure the atmospheric depolarization ratio. This design, compared with the multi-detector polarization lidar system, shows superiorities in system simplicity and stability and does not require periodical calibration. The atmospheric depolarization ratio of polarization C-DWL is obtained from the ratio of CNR of two channels, as shown in **Figure 4A, B**. The calculated atmospheric depolarization ratio is illustrated in **Figure 4C**.

Coding C-DWL

Wind field detection in high-distance resolution is one of the most essential directions of Doppler lidar. By increasing the distance resolution, DWL can be applied in the detection of aircraft wake vortices, wind tunnels, and many other special cases. Lidar based on the time-of-flight method can potentially reduce the pulse width to increase the distance resolution, while under the constraint of peak power of pulse laser energy, reducing pulse width will reduce the pulse energy, thus leading to a lower SNR.
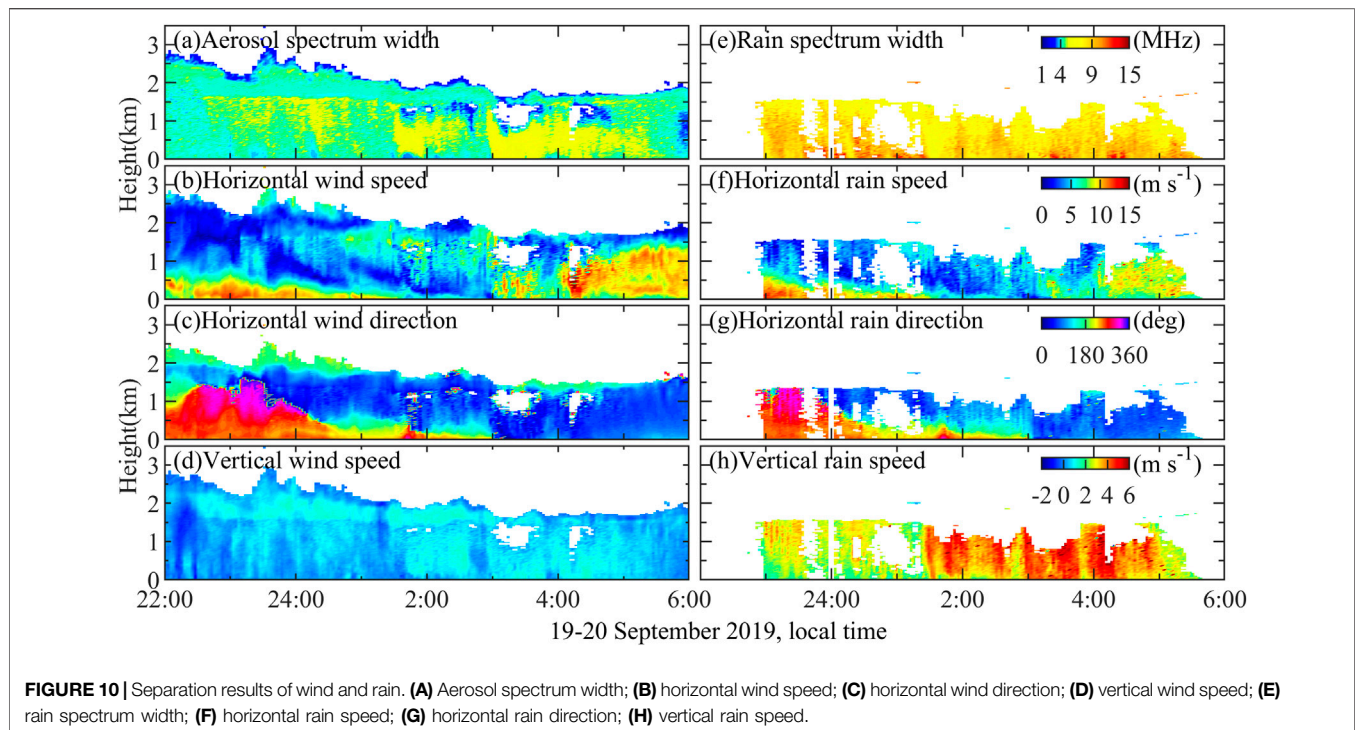
To solve that, the pulse coding technique is applied in C-DWL to increase the pulse repetition frequency without reducing the aliasing distance, and thus, the average power of the pulse is increased (Wang et al., 2019). Due to the high distance resolution, the coding system has a lower magnitude of the power spectrum, compared with a non-coding system.

Another attempt to improve the distance resolution is the DCP technique (Zhang et al., 2021). By employing pulse pair with appropriate window functions, the DCP scheme offers an approach to improve the distance resolution without broadening the spectrum width. At a laser peak power of 250 W, with a spatial and temporal resolution of 3.3 m and 1 s, continuous radial wind profiling over 700 m is realized with a maximum error of 0.1 m/s.

Atmospheric Multi-Parameter C-DWL

The output parameter of the traditional coherent lidar with a single function contains only radial wind field data. Through a depth analysis on the backscattering signal power spectrum of the coherent lidar, the CNR, spectral width, skewness, and radial speed could be obtained. Then, cloud base, the boundary layer height, rain speed, wind shear, turbulence dissipation, and many other atmospheric parameters could be inversed (Yuan et al., 2020).

A typical atmospheric multi-parameter C-DWL is applied to provide meteorological services for the 70th anniversary of China's National Day, in Inner Mongolia, China (43°54′ N, 115°58′ E) (Yuan et al., 2020). The output parameters contain CNR, spectral width, skewness, horizontal wind speed and

FIGURE 10 | Separation results of wind and rain. **(A)** Aerosol spectrum width; **(B)** horizontal wind speed; **(C)** horizontal wind direction; **(D)** vertical wind speed; **(E)** rain spectrum width; **(F)** horizontal rain speed; **(G)** horizontal rain direction; **(H)** vertical rain speed.

direction, vertical wind speed, turbulence intensity rate, and wind shear intensity, as shown in **Figure 6**. Based on those parameters, the atmospheric conditions could be well-identified. **Figure 7** shows the identification results of atmospheric conditions.

APPLICATIONS OF DWL

Through numerous deployments over the past four decades, the efficacy of DWLs for a variety of atmospheric applications has been demonstrated, including airport surveillance for low-level wind shear and wake vortex detection (Chan et al., 2006) (Dolfi-Bouteyre et al., 2009b), wind turbine control (Wu et al., 2016), atmospheric dynamics research, improvement of weather forecasts, etc. Here, three typical examples are discussed in more detail.

Atmospheric Turbulence Detection

Turbulence measurements using ground-based wind lidars are reviewed in Sathe and Mann (2013). Various parameters are used to estimate turbulence quantity using a lidar, including turbulent kinetic energy dissipation rate (TKEDR), radial velocity variance, coherence of the components of the wind field, etc. Continuous C-DWL observations of low-level jets and turbulence during September 27–28, 2019 are shown in **Figure 8** (Yuan et al., 2020). The surface turbulence is generated by the drag of the low-level jet, and the TKEDR is shown in **Figure 8G**. Convection characteristics of vertical velocity also characterize turbulence, as shown in **Figure 8F**. The cloud attenuates the solar radiation sometimes during the daytime, thus decreasing the updraft.

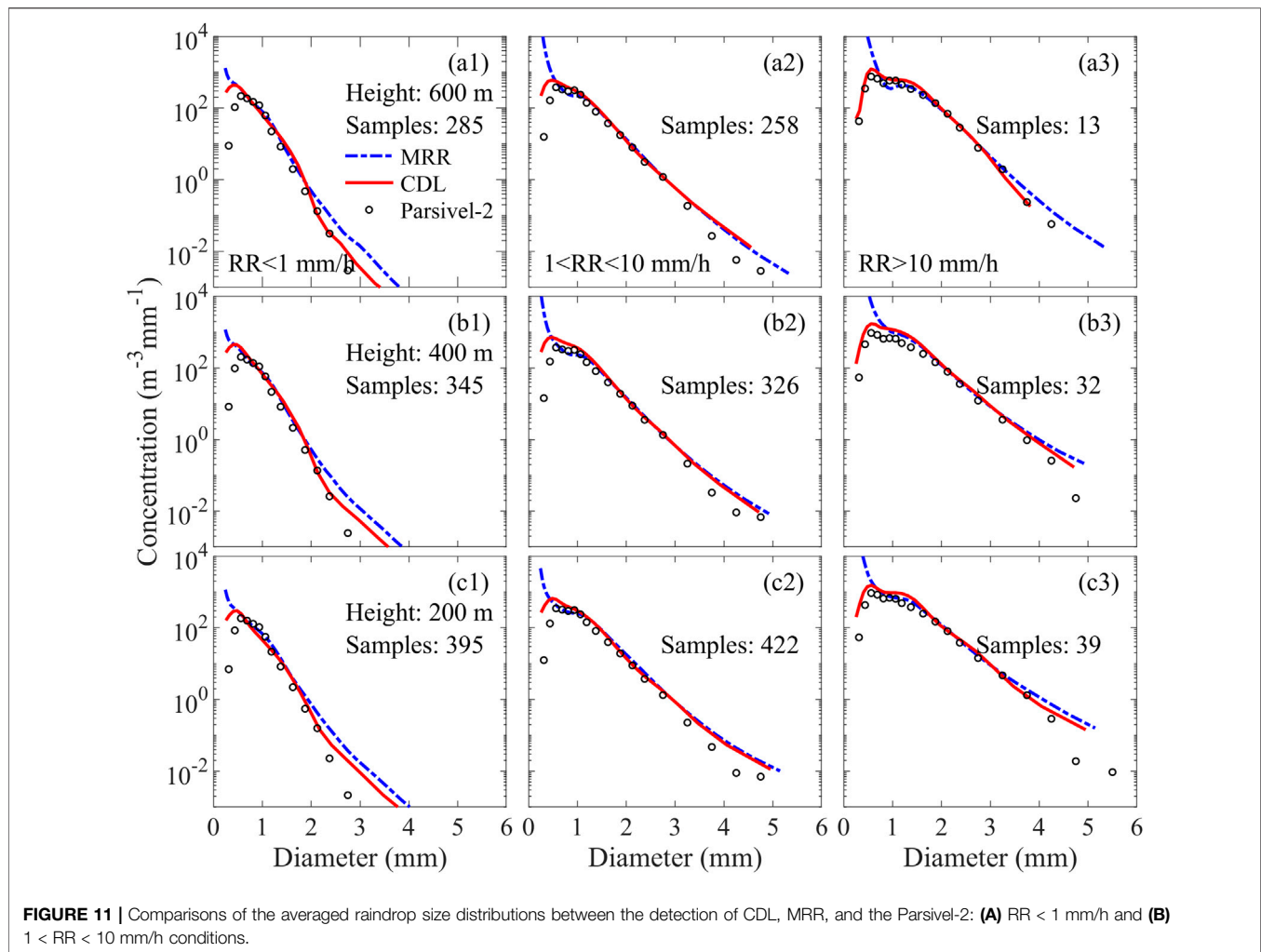Consequently, the turbulence is weakened, as shown in **Figure 8G**.

Regarding the C-DWL measurement, the atmospheric turbulence could be inversed to have an approximation of the mixed layer height. A comparison experiment was carried out between lidar with temperature control and lidar without temperature control. The results showed that the TKEDR threshold is a robust method for determining the boundary layer height, compared with the CNR threshold method (Wang et al., 2021).

Gravity Wave Detection

The atmospheric parameters (temperature, density, and wind field) are quite sensitive to the variation of the gravity wave, and the presence of gravity wave is closely related to the strong convection current events, background wind field, and disastrous weather. A long-lived GW in the ABL during a field experiment in Anqing, China (116°58′ E, 30°37′ N) is analyzed (Jia et al., 2019). Persistent GWs over 10 h with periods ranging from 10 to 30 min in the ABL within 2-km height are detected by a coherent Doppler lidar from four to five in September 2018, as shown in **Figure 9**. Based on experiments and simplified two-dimensional computational fluid dynamics numerical simulations, a reasonable generation mechanism of this persistent wave is that the wind shear around the low-level jet leads to wave generation in the condition of the light horizontal wind.

Precipitation Detection

Recently, lidars have been extended to precipitation detection, for their ability to detect the aerosol and precipitation signals

FIGURE 11 | Comparisons of the averaged raindrop size distributions between the detection of CDL, MRR, and the Parsivel-2: **(A)** RR < 1 mm/h and **(B)** 1 < RR < 10 mm/h conditions.

simultaneously under rain conditions (Brückel, 1990; Wei et al., 2019; Wei et al., 2021). By deep analysis on the power spectrum, the C-DWL can provide precise wind and rain detection with high spatial and temporal resolutions (Yuan et al., 2020). Double-peak fitting is applied to separate the aerosol and rain components in these power spectra. The separation results of wind and rain are shown in **Figure 10**.

Retrieval of the raindrop size distribution using C-DWL is still a challenging work, as both accurate backscattering cross-section at the working wavelength and reflectivity spectrum of raindrop are required. To obtain raindrop size distribution using the C-DWL, the Mie theory and the vectorial complex ray model are applied to calculate backscattering cross-section for small spherical raindrops and large oblate raindrops, and then, iterative deconvolution method is proposed to separate the reflectivity spectrum of a raindrop from the lidar power spectrum (Wei et al., 2021). The statistical result of different raindrop size spectra in different rain rates (RR) between different lidar detections is illustrated in **Figure 11** (Wei et al., 2021).

DISCUSSION AND CONCLUSION

In terms of the conclusion from the development history of DWL, the progress of DWL is summarized in the following:

✓ In the commercial view, there are many private companies with commercialized products.
✓ From gas to solid state and to all fiber, the C-DWL wavelength varies from 10.6 to 1.06, 2, and 1.5 μm. The current mainstream wavelength is 1.5 μm.
✓ Direct wind measurement lidar has advantages for global wind field acquisition by combining Mie and Rayleigh scattering.
✓ Regarding the C-DWL detection, the enhancement of the coherent detection technique improves the wind detection sensitivity and increases the distance. Limited by the aerosol concentration, the vertical detection range is set within 5-km height while applying an in-line fiber amplifier, and pump amplifier increases the laser energy potentially, thus allowing a longer vertical distance detection.

✓ Human eye safety should be guaranteed. The mature optics manufacturing, high atmospheric window transmittance, and many other superiorities of 1.5-μm laser further consolidate its leading position.

✓ In the signal-processing view, the algorithm develops from traditional Fourier transform and periodogram to JTFA, and many other algorithms draw the whole signals in time–frequency domain to improve the systematic distance resolution.

With the development of techniques in laser, manufacturing, and signal processing, the DWL could be constructed in an all-fiber structure and subsequently miniaturized and integrated. Hopefully, this review could give some inspiration, instructions, and prosecutions in the following development of DWL research.

AUTHOR CONTRIBUTIONS

HX and MS conceived the idea. MS wrote the manuscript with contributions from all co-authors. HX supervised the project. All authors contributed to the article and approved the submitted version.

REFERENCES

Abari, C. F., Chu, X., Michael Hardesty, R., and Mann, J. (2015a). A Reconfigurable All-Fiber Polarization-Diversity Coherent Doppler Lidar: Principles and Numerical Simulations. *Appl. Opt.* 54 (30), 8999–9009. doi:10.1364/ao.54.008999

Abari, C. F., Pedersen, A. T., Dellwik, E., and Mann, J. (2015b). Performance Evaluation of an All-Fiber Image-Reject Homodyne Coherent Doppler Wind Lidar. *Atmos. Meas. Tech.* 8 (10), 4145–4153. doi:10.5194/amt-8-4145-2015

Abari, C. F., Pedersen, A. T., and Mann, J. (2014). An All-Fiber Image-Reject Homodyne Coherent Doppler Wind Lidar. *Opt. Express* 22 (21), 25880–25894. doi:10.1364/oe.22.025880

Ando, T., Kameyama, S., and Hirano, Y. (2008). "All-fiber Coherent Doppler Lidar Technologies at Mitsubishi Electric Corporation," in IOP Conference Series: Earth and Environmental Science (IOP Publishing), 1, 012011. doi:10.1088/1755-1315/1/1/012011

Ångström, A., and Angstrom, A. (1929). On the Atmospheric Transmission of Sun Radiation and on Dust in the Air. *Geografiska Annaler* 11 (2), 156–166. doi:10.2307/519399

Asaka, K., Hirano, Y., Morimoto, Y., and Kasahara, K. (1998). Topical Papers on Microchip Lasers and Applications. Er,Yb:Glass Coherent Lidar Using a Microchip Laser as a Reference Optical Source. *Rev. Laser Eng.* 26 (12), 876–880. doi:10.2184/lsj.26.876

Asaka, K., Yanagisawa, T., and Hirano, Y. (2001). "1.5-um Eye-Safe Coherent Lidar System for Wind Velocity Measurement," in *Lidar Remote Sensing for Industry and Environment Monitoring* (International Society for Optics and Photonics), 321–328.

Augros, C., Tabary, P., Davrinche, D., and Schwartz, E. (2012). *Test of an X-Band Doppler Polarimetric Radar Combined with a Doppler LIDAR for Wind Shear Detection at Nice Airport.* ERAD.

Banakh, V., and Smalikho, I. (2013). *Coherent Doppler Wind Lidars in a Turbulent Atmosphere.* Artech House.

Barbaresco, F., Thobois, L., Dolfi-Bouteyre, A., Jeannin, N., Wilson, R., Valla, M., et al. (2015). *Monitoring Wind, Turbulence and Aircraft Wake Vortices by High Resolution RADAR and LIDAR Remote Sensors in All Weather Conditions.* URSI Scientific Days.

Bingöl, F. (2005). *Adapting a Doppler Laser Anemometer to Wind Energy.* Denmark: Technical University of Denmark, DTU, DK-2800 Kgs. Lyngby.

Browell, E. V., Wilkerson, T. D., and McIlrath, T. J. (1979). Water Vapor Differential Absorption Lidar Development and Evaluation. *Appl. Opt.* 18 (20), 3474–3483. doi:10.1364/ao.18.003474

Brückel, G. I. (1990). Working Groups-Land Surfaces and Boundary Layer-Team. *Scientific Rep.* 1990.

Bruneau, D., Garnier, A., Hertzog, A., and Porteneuve, J. (2004). Wind-velocity Lidar Measurements by Use of a Mach-Zehnder Interferometer, Comparison with a Fabry-Perot Interferometer. *Appl. Opt.* 43 (1), 173–182. doi:10.1364/ao.43.000173

Bu, Z.-C., Chen, S.-Y., Zhang, Y.-C., Chen, H., Guo, P., and Ge, X.-Y. (2015). Error Modeling and Analysis on Wind Speed and Direction for 2 μm Space Based Coherent Doppler LIDAR. *J. Infrared Millimeter Waves* 34 (4), 465–470.

Canat, G., Lombard, L., Durécu, A., Jolivet, V., Bourdon, P., Jetschke, S., et al. (2007). "Er-Yb-Doped LMA Fiber Structures for High Energy Amplification of Narrow Linewidth Pulses at 1.5 μm," in Conference on Lasers and Electro-Optics, CTuBB1 (Optical Society of America). doi:10.1109/cleo.2007.4452924

Cézard, N., Dolfi-Bouteyre, A., Huignard, J.-P., and Flamant, P. H. (2009). Performance Evaluation of a Dual Fringe-Imaging Michelson Interferometer for Air Parameter Measurements with a 355 Nm Rayleigh-Mie Lidar. *Appl. Opt.* 48 (12), 2321–2332. doi:10.1364/ao.48.002321

Chan, P., Shun, C., and Wu, K. (2006). "Operational LIDAR-Based System for Automatic Windshear Alerting at the Hong Kong International Airport," in 12th Conference on Aviation, Range, and Aerospace Meteorology.

Chan, P. W., and Lee, Y. F. (2012). Application of Short-Range Lidar in Wind Shear Alerting. *J. Atmos. oceanic Technol.* 29 (2), 207–220. doi:10.1175/jtech-d-11-00086.1

Changzhong, F., Songhua, W., and Bingyi, L. (2018). Research on Wind Retrieval Method of Coherent Doppler Lidar and Experimental Verification. *Chin. J. Lasers* 45 (4), 309–317. doi:10.3788/cjl201845.0410001

Chanin, M. L., Garnier, A., Hauchecorne, A., and Porteneuve, J. (1989). A Doppler Lidar for Measuring Winds in the Middle Atmosphere. *Geophys. Res. Lett.* 16 (11), 1273–1276. doi:10.1029/gl016i011p01273

Chen, Y., An, J., Wang, X., Sun, Y., Wang, Z., and Duan, J. (2017). Observation of Wind Shear during Evening Transition and an Estimation of Submicron Aerosol Concentrations in Beijing Using a Doppler Wind Lidar. *J. Meteorol. Res.* 31 (2), 350–362. doi:10.1007/s13351-017-6036-3

Collier, C. G., Davies, F., Davies, J., Pearson, G., and Hagen, M. (2008). "Doppler Radar and Lidar Observations of a Thunderstorm Outflow," in Proceedings of Fith European Conference on Radar in Meteorology and Hydrology (ERAD).

Diao, W., Liu, J., Zhu, X., Liu, Y., Zhang, X., and Chen, W. (2015). Study of All-Fiber Coherent Doppler Lidar Wind Profile Nonlinear Least Square Retrieval Method and Validation experiment. *Chin. J. Lasers* 42, 330–335. doi:10.3788/cjl201542.0914003

Dolfi-Bouteyre, A., Augère, B., Besson, C., Canat, G., Fleury, D., Gaudo, T., et al. (2008). "1.5 μm All Fiber Pulsed Lidar for Wake Vortex Monitoring," in 2008 Conference on Lasers and Electro-Optics and 2008 Conference on Quantum Electronics and Laser Science (IEEE), 1–2.

Dolfi-Bouteyre, A., Augere, B., Valla, M., Goular, D., Fleury, D., Canat, G., et al. (2009a). Aircraft Wake Vortex Study and Characterization with 1.5 Mm Fiber Doppler Lidar. *Aerospace Lab.* 1, 1–13.

Dolfi-Bouteyre, A., Canat, G., Valla, M., Augere, B., Besson, C., Goular, D., et al. (2009b). Pulsed 1.5-\$\mu\$m LIDAR for Axial Aircraft Wake Vortex Detection Based on High-Brightness Large-Core Fiber Amplifier. *IEEE J. Select. Top. Quan. Electron.* 15 (2), 441–450. doi:10.1109/jstqe.2008.2010463

Engin, D., Mathason, B., Stephen, M., Yu, A., Cao, H., Fouron, J.-L., et al. (2016). "High Energy, Narrow Linewidth 1572nm ErYb-Fiber Based MOPA for a Multi-Aperture CO_2 Trace-Gas Laser Space Transmitter," in *Fiber Lasers XIII: Technology, Systems, and Applications* (International Society for Optics and Photonics), 97282S. doi:10.1117/12.2212481

Friedman, J. S., Tepley, C. A., Castleberg, P. A., and Roe, H. (1997). Middle-atmospheric Doppler Lidar Using an Iodine-Vapor Edge Filter. *Opt. Lett.* 22 (21), 1648–1650. doi:10.1364/ol.22.001648

Fujiyoshi, Y. (2007). Visualization of Streaks, Thermals and Waves in the Atmospheric Boundary Layer. *J. Visualization* 9 (4), 359. doi:10.1007/bf03181772

Gardner, C. S., Tao, X., and Papen, G. C. (1995). Simultaneous Lidar Observations of Vertical Wind, Temperature, and Density Profiles in the Upper Mesosphere: Evidence for Nonseparability of Atmospheric Perturbation Spectra. *Geophys. Res. Lett.* 22 (20), 2877–2880. doi:10.1029/95gl02783

Gatt, P., Barr, K., and Margulis, M. (2015). "WindTracer® Evolution and Recent Measurement Results," in *Applications of Lasers for Sensing and Free Space Communications* (Optical Society of America). LT3D. 2.

Gentry, B. M., Chen, H., and Li, S. X. (2000). Wind Measurements with 355-nm Molecular Doppler Lidar. *Opt. Lett.* 25 (17), 1231–1233. doi:10.1364/ol.25.001231

Gibert, F., Dumas, A., Thobois, L., Bezombes, Y., Koch, G., Dabas, A., et al. (2012). "Afternoon Transition Turbulence Decay Revisited by Doppler Lidar," in Symposium on boundary layer and turbulence, Boston, USA.

Gottschall, J. (2013). *Galion Lidar Performance Verification*. Fraunhofer IWES.

Gottschall, J., Wolken-Möhlmann, G., and Lange, B. (2014). "About Offshore Resource Assessment with Floating Lidars with Special Respect to Turbulence and Extreme Events," in Journal of Physics: Conference Series (IOP Publishing), 555, 012043. doi:10.1088/1742-6596/555/1/012043

Hallermeyer, A., Dolfi-Bouteyre, A., Valla, M., Le Brusquet, L., Fleury, G., Thobois, L. P., et al. (2016). "Development and Assessment of a Wake Vortex Characterization Algorithm Based on a Hybrid LIDAR Signal Processing," in 8th AIAA Atmospheric and Space Environments Conference, 3272. doi:10.2514/6.2016-3272

Harris, M., Constant, G., and Ward, C. (2001). Continuous-wave Bistatic Laser Doppler Wind Sensor. *Appl. Opt.* 40 (9), 1501–1506. doi:10.1364/ao.40.001501

Hawley, J. G., Targ, R., Henderson, S. W., Hale, C. P., Kavaya, M. J., and Moerder, D. (1993). Coherent Launch-Site Atmospheric Wind Sounder: Theory and experiment. *Appl. Opt.* 32 (24), 4557–4568. doi:10.1364/ao.32.004557

Henderson, S. W., Hale, C. P., Magee, J. R., Kavaya, M. J., and Huffaker, A. V. (1991). Eye-safe Coherent Laser Radar System at 21 μm Using Tm,Ho:YAG Lasers. *Opt. Lett.* 16 (10), 773–775. doi:10.1364/ol.16.000773

Henderson, S. W., Suni, P. J. M., Hale, C. P., Hannon, S. M., Magee, J. R., Bruns, D. L., et al. (1993). Coherent Laser Radar at 2 Mu M Using Solid-State Lasers. *IEEE Trans. Geosci. Remote Sensing* 31 (1), 4–15. doi:10.1109/36.210439

Hogan, R. J., Grant, A. L. M., Illingworth, A. J., Pearson, G. N., and O'Connor, E. J. (2009). Vertical Velocity Variance and Skewness in clear and Cloud-Topped Boundary Layers as Revealed by Doppler Lidar. *Q.J.R. Meteorol. Soc.* 135 (640), 635–643. doi:10.1002/qj.413

Hu, Q., Rodrigo, P. J., and Pedersen, C. (2014). Remote Wind Sensing with a CW Diode Laser Lidar beyond the Coherence Regime. *Opt. Lett.* 39 (16), 4875–4878. doi:10.1364/ol.39.004875

Inokuchi, H., Endo, E., Ando, T., Asaka, K., Tanaka, H., and Hirano, Y. (2009a). "Development of an Airborne Wind Measurement System," in International Symposium on Photoelectronic Detection and Imaging 2009: Laser Sensing and Imaging (International Society for Optics and Photonics), 738205. doi:10.1117/12.836606

Inokuchi, H., Furuta, M., and Inagaki, T. (2014). "High Altitude Turbulence Detection Using an Airborne Doppler Lidar," in 29th Congress of the International Council of the Aeronautical Sciences (ICAS).

Inokuchi, H., Tanaka, H., and Ando, T. (2010). "Development of a Long Range Airborne Doppler Lidar," in Proceedings of 27th Congress of International Council of the Aeronautical Sciences (ICAS).

Inokuchi, H., Tanaka, H., and Ando, T. (2009b). Development of an Onboard Doppler Lidar for Flight Safety. *J. aircraft* 46 (4), 1411–1415. doi:10.2514/1.41738

Institute, A. N. S., and America, L. I. O. (2007). *American National Standard for Safe Use of Lasers*. Laser Institute of America.

Jia, M., Yuan, J., Wang, C., Xia, H., Wu, Y., Zhao, L., et al. (2019). Long-lived High-Frequency Gravity Waves in the Atmospheric Boundary Layer: Observations and Simulations. *Atmos. Chem. Phys.* 19 (24), 15431–15446. doi:10.5194/acp-19-15431-2019

Jiang, P., Yuan, J., Wu, K., Wang, L., and Xia, H. (2021). Turbulence Detection in the Atmospheric Boundary Layer Using Coherent Doppler Wind Lidar and Microwave Radiometer. *Atmos. Meas. Tech. Discuss.*, 1–22. doi:10.5194/amt-2021-288

Jørgensen, H. E., Mikkelsen, T., Mann, J., Bryce, D., Coffey, A., Harris, M., et al. (2004). "Site Wind Field Determination Using a CW Doppler LIDAR-Comparison with Cup Anemometers at Risø," in Special topic conference: The science of making torque from wind (Delft University of Technology), 261–266.

Kameyama, S., Ando, T., Asaka, K., Hirano, Y., and Wadaka, S. (2007). Compact All-Fiber Pulsed Coherent Doppler Lidar System for Wind Sensing. *Appl. Opt.* 46 (11), 1953–1962. doi:10.1364/ao.46.001953

Kameyama, S., Sakimura, T., Watanabe, Y., Ando, T., Asaka, K., Tanaka, H., et al. (2012). "Wind Sensing Demonstration of More Than 30km Measurable Range with a 1.5 μm Coherent Doppler Lidar Which Has the Laser Amplifier Using Er, Yb: Glass Planar Waveguide," in *Lidar Remote Sensing for Environmental Monitoring XIII* (International Society for Optics and Photonics), 85260E. doi:10.1117/12.977330

Kameyama, S., Yanagisawa, T., Ando, T., Sakimura, T., Tanaka, H., Furuta, M., et al. (2013). "Development of Wind Sensing Coherent Doppler Lidar at Mitsubishi Electric Corporation from Late 1990s to 2013," in Abstracts Int. Coherent Laser Radar Conf.

Kane, T. J., Byvik, C. E., Kozlovsky, W. J., and Byer, R. L. (1987). Coherent Laser Radar at 106 μm Using Nd:YAG Lasers. *Opt. Lett.* 12 (4), 239–241. doi:10.1364/ol.12.000239

Karlsson, C. J., Olsson, F. Å. A., Letalick, D., and Harris, M. (2000). All-fiber Multifunction Continuous-Wave Coherent Laser Radar at 155 Mm for Range, Speed, Vibration, and Wind Measurements. *Appl. Opt.* 39 (21), 3716–3726. doi:10.1364/ao.39.003716

Kavaya, M. J., Beyon, J. Y., Koch, G. J., Petros, M., Petzar, P. J., Singh, U. N., et al. (2014). The Doppler Aerosol Wind (DAWN) Airborne, Wind-Profiling Coherent-Detection Lidar System: Overview and Preliminary Flight Results. *J. Atmos. Oceanic Tech.* 31 (4), 826–842. doi:10.1175/jtech-d-12-00274.1

Kavaya, M. J., Henderson, S. W., Magee, J. R., Hale, C. P., and Huffaker, R. M. (1989). Remote Wind Profiling with a Solid-State Nd:YAG Coherent Lidar System. *Opt. Lett.* 14 (15), 776–778. doi:10.1364/ol.14.000776

Kigle, S. (2017). *Wake Identification and Characterization of a Full Scale Wind Energy Converter in Complex Terrain with Scanning Doppler Wind Lidar Systems*. Ludwig-Maximilians-Universität München.

Krueger, D. A., She, C.-Y., and Yuan, T. (2015). Retrieving Mesopause Temperature and Line-Of-Sight Wind from Full-Diurnal-Cycle Na Lidar Observations. *Appl. Opt.* 54 (32), 9469–9489. doi:10.1364/ao.54.009469

Li, D., Zheng, Y., Pan, J., Xie, Y., and Dong, G. (2010). Index System of Coherent Doppler Wind Lidar. *Opt. Tech.* 36 (6), 880–884.

Li, T., Ban, C., Fang, X., Li, J., Wu, Z., Feng, W., et al. (2018). Climatology of Mesopause Region Nocturnal Temperature, Zonal Wind and Sodium Density Observed by Sodium Lidar over Hefei, China (32° N, 117° E). *Atmos. Chem. Phys.* 18 (16), 11683–11695. doi:10.5194/acp-18-11683-2018

Li, T., Fang, X., Liu, W., Gu, S.-Y., and Dou, X. (2012). Narrowband Sodium Lidar for the Measurements of Mesopause Region Temperature and Wind. *Appl. Opt.* 51 (22), 5401–5411. doi:10.1364/ao.51.005401

Liu, J., Zhu, X., Diao, W., Liu, Y., Bi, D., Zhang, X., et al. (2012). "Development of All-Fiber Coherent Doppler Lidar to Measure Atmosphere Wind Speed," in *Optical Instrumentation for Energy and Environmental Applications* (Optical Society of America). ET4D. 1. doi:10.1364/e2.2012.et4d.1

Liu, Z.-S., Wu, D., Liu, J.-T., Zhang, K.-L., Chen, W.-B., Song, X.-Q., et al. (2002). Low-altitude Atmospheric Wind Measurement from the Combined Mie and Rayleigh Backscattering by Doppler Lidar with an Iodine Filter. *Appl. Opt.* 41 (33), 7079–7086. doi:10.1364/ao.41.007079

Lombard, L., Dolfi-Bouteyre, A., Besson, C., Augère, B., Bourdon, P., Durécu, A., et al. (2015a). "Long Range Wind Lidars Based on Novel High Spectral Brilliance All-Fibered Sources," in *Lidar Technologies, Techniques, and Measurements for Atmospheric Remote Sensing XI* (International Society for Optics and Photonics), 96450B. doi:10.1117/12.2197350

Lombard, L., Valla, M., Planchat, C., Goular, D., Augère, B., Bourdon, P., et al. (2015b). Eyesafe Coherent Detection Wind Lidar Based on a Beam-Combined Pulsed Laser Source. *Opt. Lett.* 40 (6), 1030–1033. doi:10.1364/ol.40.001030

Lux, O., Lemmerz, C., Weiler, F., Marksteiner, U., Witschas, B., Rahm, S., et al. (2018). Airborne Wind Lidar Observations over the North Atlantic in 2016 for the Pre-launch Validation of the Satellite mission Aeolus. *Atmos. Meas. Tech.* 11 (6), 3297–3322. doi:10.5194/amt-11-3297-2018

Lux, O., Lemmerz, C., Weiler, F., Marksteiner, U., Witschas, B., Reitebuch, O., et al. (2019). *Aeolus-ESA's Wind Lidar Mission: Overview and First Results.*

Marinov, V. S., Stoyanov, D. V., Naboko, V. N., and Naboko, S. V. (1996). "Performance of 10.6 um CO2 Doppler lidar at low-laser-frequency stability using a fixed hard target," in *Ninth International School on Quantum Electronics: Lasers–Physics and Applications* (International Society for Optics and Photonics), 288–293.

McKay, J. A. (2002). Assessment of a Multibeam Fizeau Wedge Interferometer for Doppler Wind Lidar. *Appl. Opt.* 41 (9), 1760–1767. doi:10.1364/ao.41.001760

Newsom, R. K., and Banta, R. M. (2003). Shear-flow Instability in the Stable Nocturnal Boundary Layer as Observed by Doppler Lidar during CASES-99. *J. Atmos. Sci.* 60 (1), 16–33. doi:10.1175/1520-0469(2003)060<0016:sfiits>2.0.co;2

North, G. R., Pyle, J. A., and Zhang, F. (2014). *Encyclopedia of Atmospheric Sciences.* Elsevier.

O'Connor, E. J., Illingworth, A. J., Brooks, I. M., Westbrook, C. D., Hogan, R. J., Davies, F., et al. (2010). A Method for Estimating the Turbulent Kinetic Energy Dissipation Rate from a Vertically Pointing Doppler Lidar, and Independent Evaluation from Balloon-Borne *In Situ* Measurements. *J. Atmos. oceanic Technol.* 27 (10), 1652–1664.

Paffrath, U., Lemmerz, C., Reitebuch, O., Witschas, B., Nikolaus, I., and Freudenthaler, V. (2009). The Airborne Demonstrator for the Direct-Detection Doppler Wind Lidar ALADIN on ADM-Aeolus. Part II: Simulations and Rayleigh Receiver Radiometric Performance. *J. Atmos. Oceanic Tech.* 26 (12), 2516–2530. doi:10.1175/2009jtecha1314.1

Pan, J., Qin, S., and Liu, G. (2013). Coherent Laser Wind Measurement Radar Wind Field Measurement Technology. *Infrared Laser Eng.* 42 (7), 1720–1724.

Pearson, G. N., Ridley, K. D., and Willetts, D. V. (2005). "Long Range 3D Active Imagery with a Scanned Single Element 1.5 μm Coherent Lidar System," in *Electro-Optical Remote Sensing* (International Society for Optics and Photonics), 59880M. doi:10.1117/12.632788

Pearson, G. N., Roberts, P. J., Eacock, J. R., and Harris, M. (2002). Analysis of the Performance of a Coherent Pulsed Fiber Lidar for Aerosol Backscatter Applications. *Appl. Opt.* 41 (30), 6442–6450. doi:10.1364/ao.41.006442

Pedersen, A. T., Abari, C. F., Mann, J., and Mikkelsen, T. (2014). "Theoretical and Experimental Signal-To-Noise Ratio Assessment in New Direction Sensing Continuous-Wave Doppler Lidar," in Journal of Physics: Conference Series (IOP Publishing), 524, 012004. doi:10.1088/1742-6596/524/1/012004

Philippov, V. N., Sahu, J. K., Codemard, C. A., Clarkson, W. A., Jang, J. N., Nilsson, J., et al. (2004). "All-fiber 1.15-mJ Pulsed Eye-Safe Optical Source," in *Fiber Lasers: Technology, Systems, and Applications* (International Society for Optics and Photonics), 1–7. doi:10.1117/12.527451

Phillips, M. W., Hannon, S. M., Henderson, S. W., Gatt, P., and Huffaker, R. M. (1997). "Solid-state Coherent Lidar Technology for Space-Based Wind Measurement," in *Optics in Atmospheric Propagation, Adaptive Systems, and Lidar Techniques for Remote Sensing* (International Society for Optics and Photonics), 68–75. doi:10.1117/12.263153

Prasad, N. S., Tracy, A., Vetorino, S., Higgins, R., and Sibell, R. (2016). "Innovative Fiber-Laser Architecture-Based Compact Wind Lidar," in *Photonic Instrumentation Engineering III* (International Society for Optics and Photonics), 97540J. doi:10.1117/12.2218226

Proctor, F., and Hamilton, D. (2009). "Evaluation of Fast-Time Wake Vortex Prediction Models," in 47th AIAA Aerospace Sciences Meeting including The New Horizons Forum and Aerospace Exposition, 344. doi:10.2514/6.2009-344

Rees, D., Vyssogorets, M., Meredith, N. P., Griffin, E., and Chaxell, Y. (1996). The Doppler Wind and Temperature System of the ALOMAR Lidar Facility: Overview and Initial Results. *J. Atmos. Terrestrial Phys.* 58 (16), 1827–1842. doi:10.1016/0021-9169(95)00174-3

Reitebuch, O., and Hardesty, R. M. (2021). "Doppler Wind Lidar," in *Springer Handbook of Atmospheric Measurements* (Springer), 759–797. doi:10.1007/978-3-030-52171-4_27

Reitebuch, O., Lemmerz, C., Nagel, E., Paffrath, U., Durand, Y., Endemann, M., et al. (2009). The Airborne Demonstrator for the Direct-Detection Doppler Wind Lidar ALADIN on ADM-Aeolus. Part I: Instrument Design and Comparison to Satellite Instrument. *J. Atmos. Oceanic Tech.* 26 (12), 2501–2515. doi:10.1175/2009jtecha1309.1

Reitebuch, O. (2012). "The Spaceborne Wind Lidar mission ADM-Aeolus," in *Atmospheric Physics* (Springer), 815–827. doi:10.1007/978-3-642-30183-4_49

Renard, W., Goular, D., Valla, M., Planchat, C., Augère, B., Dolfi-Bouteyre, A., et al. (2014). "Beyond 10 Km Range Wind-Speed Measurement with a 1.5 Mm All-Fiber Laser Source," in *CLEO: Applications and Technology* (Optical Society of America). AW1P. 5.

Rodrigo, P. J., and Pedersen, C. (2012). "Comparative Study of the Performance of Semiconductor Laser Based Coherent Doppler Lidars," in *High-Power Diode Laser Technology and Applications X* (International Society for Optics and Photonics), 824112. doi:10.1117/12.908800

Sakimura, T., Watanabe, Y., Ando, T., Kameyama, S., Asaka, K., Tanaka, H., et al. (2013). "3.2 mJ, 1.5 μm Laser Power Amplifier Using an Er, Yb: Glass Planar Waveguide for a Coherent Doppler LIDAR," in Proc 17th Coherent Laser Radar Conference.

Sathe, A., and Mann, J. (2013). A Review of Turbulence Measurements Using Ground-Based Wind Lidars. *Atmos. Meas. Tech.* 6 (11), 3147–3167. doi:10.5194/amt-6-3147-2013

Shangguan, M.-J., Xia, H.-Y., Dou, X.-K., Wang, C., Qiu, J.-W., Zhang, Y.-P., et al. (2015). Comprehensive Wind Correction for a Rayleigh Doppler Lidar from Atmospheric Temperature and Pressure Influences and Mie Contamination. *Chin. Phys. B* 24 (9), 094212. doi:10.1088/1674-1056/24/9/094212

Shangguan, M., Xia, H., Wang, C., Qiu, J., Lin, S., Dou, X., et al. (2017). Dual-frequency Doppler Lidar for Wind Detection with a Superconducting Nanowire Single-Photon Detector. *Opt. Lett.* 42 (18), 3541–3544. doi:10.1364/ol.42.003541

Shangguan, M., Xia, H., Wang, C., Qiu, J., Shentu, G., Zhang, Q., et al. (2016). All-fiber Upconversion High Spectral Resolution Wind Lidar Using a Fabry-Perot Interferometer. *Opt. Express* 24 (17), 19322–19336. doi:10.1364/oe.24.019322

She, C. Y., Vance, J. D., Williams, B. P., Krueger, D. A., Moosmüller, H., Gibson-Wilde, D., et al. (2002). Lidar Studies of Atmospheric Dynamics Near Polar Mesopause. *Eos Trans. AGU* 83 (27), 289–293. doi:10.1029/2002eo000206

She, C. Y., and Yu, J. R. (1994). Simultaneous Three-Frequency Na Lidar Measurements of Radial Wind and Temperature in the Mesopause Region. *Geophys. Res. Lett.* 21 (17), 1771–1774. doi:10.1029/94gl01417

Smith, D. A., Harris, M., Coffey, A. S., Mikkelsen, T., Jørgensen, H. E., Mann, J., et al. (2006). Wind Lidar Evaluation at the Danish Wind Test Site in Høvsøre. *Wind Energ. Int. J. Prog. Appl. Wind Power Convers. Tech.* 9 (1-2), 87–93. doi:10.1002/we.193

Spuler, S. M., Richter, D., Spowart, M. P., and Rieken, K. (2011). Optical Fiber-Based Laser Remote Sensor for Airborne Measurement of Wind Velocity and Turbulence. *Appl. Opt.* 50 (6), 842–851. doi:10.1364/ao.50.000842

Stoffelen, A., Marseille, G.-J., and Barkmeijer, J. (2005). "Sensitivity Approach to Study Doppler Wind Lidar Sampling Requirements for Extreme Weather Prediction," in Proc. Winds Workshop, Citeseer, 42.

Suni, P. J. M., and Henderson, S. W. (1991). 1-mJ/pulse Tm:YAG Laser Pumped by a 3-W Diode Laser. *Opt. Lett.* 16 (11), 817–819. doi:10.1364/ol.16.000817

Targ, R., Steakley, B. C., Hawley, J. G., Ames, L. L., Forney, P., Swanson, D., et al. (1996). Coherent Lidar Airborne Wind Sensor II: Flight-Test Results at 2 and 10 μm. *Appl. Opt.* 35 (36), 7117–7127. doi:10.1364/ao.35.007117

Tepley, C. A. (1994). Neutral Winds of the Middle Atmosphere Observed at Arecibo Using a Doppler Rayleigh Lidar. *J. Geophys. Res.* 99 (D12), 25781–25790. doi:10.1029/94jd02213

Thobois, L., Loaec, S., Boquet, M., Krishna, R., Murthy, J., Cariou, P., et al. (2014). "Recent Developments of Windcube Doppler Lidars for Airport Wind Hazards Monitoring," in *WakeNet-Eu 2014 Workshop*.

Thobois, L. P., Krishnamurthy, R., Loaec, S., Cariou, J. P., Dolfi-Bouteyre, A., and Valla, M. (2015). "Wind and EDR Measurements with Scanning Doppler LIDARs for Preparing Future Weather Dependent Separation Concepts," in *7th AIAA Atmospheric and Space Environments Conference*, 3317.

Wang, C., Xia, H., Liu, Y., Lin, S., and Dou, X. (2018). Spatial Resolution Enhancement of Coherent Doppler Wind Lidar Using Joint Time-Frequency Analysis. *Opt. Commun.* 424, 48–53. doi:10.1016/j.optcom.2018.04.042

Wang, C., Xia, H., Shangguan, M., Wu, Y., Wang, L., Zhao, L., et al. (2017). 15 μm Polarization Coherent Lidar Incorporating Time-Division Multiplexing. *Opt. Express* 25 (17), 20663–20674. doi:10.1364/oe.25.020663

Wang, C., Xia, H., Wu, Y., Dong, J., Wei, T., Wang, L., et al. (2019). Meter-scale Spatial-Resolution-Coherent Doppler Wind Lidar Based on Golay Coding. *Opt. Lett.* 44 (2), 311–314. doi:10.1364/ol.44.000311

Wang, H., Barthelmie, R. J., Crippa, P., Doubrawa, P., and Pryor, S. C. (2014). "Profiles of Wind and Turbulence in the Coastal Atmospheric Boundary Layer of Lake Erie," in Journal of Physics: Conference Series (IOP Publishing), 524, 012117. doi:10.1088/1742-6596/524/1/012117

Wang, L., Qiang, W., Xia, H., Wei, T., Yuan, J., and Jiang, P. (2021). Robust Solution for Boundary Layer Height Detections with Coherent Doppler Wind Lidar. *Adv. Atmos. Sci.* 38 (11), 1920–1928. doi:10.1007/s00376-021-1068-0

Wei, T., Xia, H., Hu, J., Wang, C., Shangguan, M., Wang, L., et al. (2019). Simultaneous Wind and Rainfall Detection by Power Spectrum Analysis Using a VAD Scanning Coherent Doppler Lidar. *Opt. Express* 27 (22), 31235–31245. doi:10.1364/oe.27.031235

Wei, T., Xia, H., Wu, Y., Yuan, J., Wang, C., and Dou, X. (2020). Inversion Probability Enhancement of All-Fiber CDWL by Noise Modeling and Robust Fitting. *Opt. Express* 28 (20), 29662–29675. doi:10.1364/oe.401054

Wei, T., Xia, H., Yue, B., Wu, Y., and Liu, Q. (2021). Remote Sensing of Raindrop Size Distribution Using the Coherent Doppler Lidar. *Opt. Express* 29 (11), 17246–17257. doi:10.1364/oe.426326

Weifeng Diao, W. D., Xin Zhang, X. Z., Jiqiao Liu, J. L., Xiaopeng Zhu, X. Z., Yuan Liu, Y. L., Decang Bi, D. B., et al. (2014). All Fiber Pulsed Coherent Lidar Development for Wind Profiles Measurements in Boundary Layers. 中国光学快报 12 (7), 072801–072804. doi:10.3788/col201412.072801

Weitkamp, C. (2006). *Lidar: Range-Resolved Optical Remote Sensing of the Atmosphere*. Springer Science & Business.

Werner, C. (2005). "Doppler Wind Lidar," in *Lidar* (Springer), 325–354.

Westbrook, C. D., Illingworth, A. J., O'Connor, E. J., and Hogan, R. J. (2010). Doppler Lidar Measurements of Oriented Planar Ice Crystals Falling from Supercooled and Glaciated Layer Clouds. *Q.J.R. Meteorol. Soc.* 136 (646), 260–276. doi:10.1002/qj.528

Wu, S., Liu, B., Liu, J., Zhai, X., Feng, C., Wang, G., et al. (2016). Wind Turbine Wake Visualization and Characteristics Analysis by Doppler Lidar. *Opt. Express* 24 (10), A762–A780. doi:10.1364/oe.24.00a762

Wu, S., Sun, D., and Liu, Z. (2003). "Frequency Locking of Diode-Pumped Nd: YAG Lasers with the Digital PID Method at 532-nm Iodine Lines in Incoherent Wind Lidar," in *Lidar Remote Sensing for Industry and Environment Monitoring III* (International Society for Optics and Photonics), 348–353. doi:10.1117/12.466460

Wu, S., Sun, K., Dai, G., Wang, X., Liu, X., Liu, B., et al. (2021). Inter-comparison of Wind Measurements in the Atmospheric Boundary Layer with Aeolus and a Ground-Based Coherent Doppler Lidar Network over China. *Atmos. Meas. Tech. Discuss.*, 1–26. doi:10.5194/amt-2021-260

Wu, S., Yin, J., Liu, B., Liu, J., Li, R., Wang, X., et al. (2014). "Characterization of Turbulent Wake of Wind Turbine by Coherent Doppler Lidar," in *Lidar Remote Sensing for Environmental Monitoring XIV* (International Society for Optics and Photonics), 92620H. doi:10.1117/12.2069566

Wulfmeyer, V., Randall, M., Brewer, A., and Hardesty, R. M. (2000). 2-μm Doppler Lidar Transmitter with High Frequency Stability and Low Chirp. *Opt. Lett.* 25 (17), 1228–1230. doi:10.1364/ol.25.001228

Xia, H., Dou, X., Shangguan, M., Zhao, R., Sun, D., Wang, C., et al. (2014). Stratospheric Temperature Measurement with Scanning Fabry-Perot Interferometer for Wind Retrieval from mobile Rayleigh Doppler Lidar. *Opt. Express* 22 (18), 21775–21789. doi:10.1364/oe.22.021775

Xia, H., Dou, X., Sun, D., Shu, Z., Xue, X., Han, Y., et al. (2012). Mid-altitude Wind Measurements with mobile Rayleigh Doppler Lidar Incorporating System-Level Optical Frequency Control Method. *Opt. Express* 20 (14), 15286–15300. doi:10.1364/oe.20.015286

Xia, H., Shangguan, M., Wang, C., Shentu, G., Qiu, J., Zhang, Q., et al. (2016). Micro-pulse Upconversion Doppler Lidar for Wind and Visibility Detection in the Atmospheric Boundary Layer. *Opt. Lett.* 41 (22), 5218–5221. doi:10.1364/ol.41.005218

Xia, H., Shentu, G., Shangguan, M., Xia, X., Jia, X., Wang, C., et al. (2015). Long-range Micro-pulse Aerosol Lidar at 15 μm with an Upconversion Single-Photon Detector. *Opt. Lett.* 40 (7), 1579–1582. doi:10.1364/ol.40.001579

Xia, H., Sun, D., Yang, Y., Shen, F., Dong, J., and Kobayashi, T. (2007). Fabry-Perot Interferometer Based Mie Doppler Lidar for Low Tropospheric Wind Observation. *Appl. Opt.* 46 (29), 7120–7131. doi:10.1364/ao.46.007120

Xia, Y., Du, L., Cheng, X., Li, F., Wang, J., Wang, Z., et al. (2017). Development of a Solid-State Sodium Doppler Lidar Using an All-Fiber-Coupled Injection Seeding Unit for Simultaneous Temperature and Wind Measurements in the Mesopause Region. *Opt. Express* 25 (5), 5264–5278. doi:10.1364/oe.25.005264

Yanagisawa, T., Asaka, K., Hamazu, K., and Hirano, Y. (2001). 11-mJ, 15-Hz Single-Frequency Diode-Pumped Q-Switched Er, Yb:phosphate Glass Laser. *Opt. Lett.* 26 (16), 1262–1264. doi:10.1364/ol.26.001262

Yu, C., Shangguan, M., Xia, H., Zhang, J., Dou, X., and Pan, J.-W. (2017). Fully Integrated Free-Running InGaAs/InP Single-Photon Detector for Accurate Lidar Applications. *Opt. Express* 25 (13), 14611–14620. doi:10.1364/oe.25.014611

Yu, S., Zhang, Z., Xia, H., Dou, X., Wu, T., Hu, Y., et al. (2021). Photon-counting Distributed Free-Space Spectroscopy. *Light: Sci. Appl.* 10 (1), 1–10. doi:10.1038/s41377-021-00650-2

Yuan, J., Xia, H., Wei, T., Wang, L., Yue, B., and Wu, Y. (2020). Identifying Cloud, Precipitation, Windshear, and Turbulence by Deep Analysis of the Power Spectrum of Coherent Doppler Wind Lidar. *Opt. Express* 28 (25), 37406–37418. doi:10.1364/oe.412809

Zhai, X., Wu, S., and Liu, B. (2017). Doppler Lidar Investigation of Wind Turbine Wake Characteristics and Atmospheric Turbulence under Different Surface Roughness. *Opt. Express* 25 (12), A515–A529. doi:10.1364/oe.25.00a515

Zhang, Y., Wu, Y., and Xia, H. (2021). Spatial Resolution Enhancement of Coherent Doppler Wind Lidar Using Differential Correlation Pair Technique. *Opt. Lett.* 46 (22), 5550–5553. doi:10.1364/ol.442121